Combination of Langmuir-Hinshelwood-Hougen-Watson and microkinetic approaches for simulation of biogas dry reforming over a platinum-rhodium alumina catalyst

Sawatmongkhon, Boonlue; Theinnoi, Kampanart; Wongchang; Haoharn; Tsolakis, Athanasios

DOI:
10.1016/j.ijhydene.2017.08.048

Document Version
Peer reviewed version

Citation for published version (Harvard):
Sawatmongkhon, B, Theinnoi, K, Wongchang, Haoharn, & Tsolakis, A 2017, 'Combination of Langmuir-Hinshelwood-Hougen-Watson and microkinetic approaches for simulation of biogas dry reforming over a platinum-rhodium alumina catalyst', *International Journal of Hydrogen Energy*, vol. 42, no. 39, pp. 24697-24712. https://doi.org/10.1016/j.ijhydene.2017.08.048

Combination of Langmuir-Hinshelwood-Hougen-Watson and microkinetic approaches for simulation of biogas dry reforming over a platinum-rhodium alumina catalyst

B. Sawatmongkhon[a,b,*], K. Theinnoi[a,b], T. Wongchang[a,b], C. Haoharn[a,b], A. Tsolakis[c]

[a] College of Industrial Technology, King Mongkut's University of Technology North Bangkok, 1518 Pracharat 1 Road, Wongsawang, Bangsue, Bangkok, 10800, Thailand.

[b] Research Centre for Combustion Technology and Alternative Energy (CTAE), Science and Technology Research Institute, King Mongkut's University of Technology North Bangkok, Thailand.

[c] School of Engineering, Mechanical and Manufacturing Engineering, University of Birmingham, Birmingham B15 2TT, UK.

Abstract

Dry reforming of CH_4 on a platinum-rhodium alumina catalyst is selected to numerically investigate biogas reforming process. Langmuir-Hinshelwood-Hougen-Watson (LHHW) rate expressions for dry reforming and reverse water-gas shift reactions are presented. Activation energies are estimated by combining microkinetics with the theory of unity bond index-quadratic exponential potential (UBI-QEP). Pre-exponential factors are initially obtained by using the transition state theory (TST) and optimised, later, by minimising errors between modelling and experimental data. Adsorption of CH_4 on the catalyst surface is found to be the rate determining step in the range of relatively low temperature (600 - 770 °C), while at relatively high temperature (770 - 950 °C) the thermal cracking of adsorbed CH_4 is the rate controlling step. Small effect of reverse water-gas shift reaction results in the ratio of H_2 to CO produced less than unity for all operating conditions. The simulation shows that the dry reforming process proceeds with reaction rate far from equilibrium state. The presented mechanism is capable of predicting the dependence of biogas dry reforming activities (e.g., reactant conversions, product formations, H_2 to CO ratio, and temperature profile inside the catalyst) on operating conditions (e.g., inlet temperature, heat supplied through the catalyst wall, and composition of biogas at inlet).

Keywords: Biogas dry reforming, Langmuir-Hinshelwood-Hougen-Watson approach, Microkinetics, On-board hydrogen production

1. Introduction

Hydrogen (H_2) has been deemed as one of the future energy vectors for transportation~~,~~. Together with an oxidising agent and fuel cell, it can be used to produce electricity for an electric vehicle with zero emission. ~~in~~ In addition ~~to,~~ its importance in the field of automotive catalytic aftertreatment systems is paramount. In a NO_x reduction system of a diesel engine, such as hydrocarbon selective catalytic reduction (HC-SCR), a small amount of hydrogen is used as an ideal co-feeder in order to decrease the minimum temperature needed to drive the NO_x removal process [1–4]. In terms of particulate matter (PM) control, hydrogen promotes the formation of NO_2 which is more active than oxygen to oxidise the PM at low temperatures in the regeneration step [5]. Furthermore, hydrogen utilisation in engines for combustion also enhances auto-ignition of some alternative hydrocarbon fuels [6] and breaks the PM-NO_x trade-off [7–10]. Moreover, the potential of hydrogen on performance of a gasoline direct injection (GDI) engine was carefully investigated. With hydrogen-rich reformate exhaust gas recirculation (REGR), Tsolakis and co-workers found that 1) the indicated engine efficiency was improved; 2) the dilution limit was extended; 3) NO_x emission was dropped; 4) knock was reduced; 5) particulate matter emissions in both mass and number were declined; 6) combustion stability inside the cylinder increased due to high diffusivity and flame speed of hydrogen; and 7) spark timing can be retarded which enhanced the available time for fuel-air mixture [11–13]. Also, hydrogen and carbon monoxide (CO) (also called syngas) are the main source for ~~production~~synthesis of liquid hydrocarbons via the Fischer-Tropsch process, methanol ~~alcohol~~, and fine chemicals.

Biogas is an alternative and renewable energy vector. It is easily produced by the biological breakdown of organic matter in which oxygen is absent. Biogas mainly consists of methane (CH_4) and carbon dioxide (CO_2). Normally, the volumetric fraction of CH_4 and CO_2 varies from 50 to 75% and from 50 to 25%, respectively. Biogas used directly in an internal combustion engine is a challenging task because the high content of CO_2 reduces the fuel calorific value. To employ biogas in automotive applications, biogas has to be upgraded to

syngas ~~(e.g., hydrogen (H_2) and carbon monoxide (CO))~~ by using fuel reforming processes [14–17]. The reforming of methane including dry reforming, partial oxidation, steam reforming, water-gas shift, and complete combustion is given below:

Dry reforming

$CH_4 + CO_2 \rightarrow 2CO + 2H_2$ $\Delta h_R = +260.62$ kJ/mol

Partial oxidation

$CH_4 + 0.5O_2 \rightarrow CO + 2H_2$ $\Delta h_R = -22.63$ kJ/mol

Steam reforming

$CH_4 + H_2O \rightarrow CO + 3H_2$ $\Delta h_R = +226.81$ kJ/mol

Water-gas shift

$CO + H_2O \rightarrow CO_2 + H_2$ $\Delta h_R = -33.86$ kJ/mol

Complete combustion

$CH_4 + 2O_2 \rightarrow CO_2 + 2H_2O$ $\Delta h_R = -891.64$ kJ/mol

Dry or CO_2 reforming was found to be the major step for the partial oxidation of methane over supported platinum catalysts [18]. First, part of methane is converted to CO_2 and H_2O by the complete combustion process; then, the produced CO_2 and H_2O reacted with the remaining methane to form syngas through dry and steam reforming paths, respectively. The reverse water gas shift (RWGS) was one of chemical reactions taking place during dry reforming of methane over Pt/PrCeZrO [19] and Ni-Co/CeO_2 [20] catalysts. Part of the H_2 produced by the dry reforming was consumed by CO_2 to generate CO and H_2O. So, the ratio of H_2 to CO was always less than unity. Wang et al. [21] suggested that an equimolar amount of H_2 and CO was found at the CH_4 to CO_2 ratio of 2. The authors also proposed that carbon deposited on the Ni catalyst was generated from both CH_4 and CO_2. On the one hand, the adsorbed carbon chemically reacted with surface oxygen to produce adsorbed CO. On the other hand, the carbon was permanently stuck on the catalyst surface and caused the catalyst deactivation. Carbon derived from CO_2 was the main path for the catalyst coking. Highly active surface carbon was

created from the thermal cracking of CH_4. Then, the active carbon was rapidly consumed by CO_2 via the reverse Boudouard reaction. However, O'Connor et al. [22] studied transient CO_2 reforming of CH_4 over Pt/ZrO_2 and Pt/Al_2O_3 catalysts and found that more than 99% of carbon accumulated on both catalysts was derived from the CH_4 molecule. CH_4 decomposition that formed carbon, took place over platinum sites in both catalysts. The difference between the two catalysts was that the Pt/ZrO_2 catalyst was able to dissociate CO_2 in the absence of CH_4 while over the Pt/Al_2O_3 catalyst, the CO_2 dissociation is assisted by hydrogen derived from CH_4. Moreover, in contrast to what has been observed over Ni and Ru catalysts, the direct reaction between CO_2 and adsorbed carbon (the reverse Boudouard reaction) was a small effect and can be excluded. The authors recommended that the CO_2 dissociation was the slowest step for the CO_2 reforming over the platinum supported catalysts. In cases of catalyst stability, non-noble metals (e.g., Fe, Co, and Ni) are easily lost activity with a short time. Rhodium (Rh) is considered as the most suitable catalyst in the methane dry reforming reaction. Low dissociation enthalpies of methane made Rh appropriate in terms of activity and stability [23]. As a support of Pt catalyst, CeO_2 showed highest stability comparing to Al_2O_3, ZrO_2, and Y_2O_3 for the partial oxidation of methane. Due to higher reducibility and oxygen storage/release capacity, CeO_2 was able to continuously remove carbon deposited on active sites [18].

Numerical simulation together with catalytic reaction models formed based on either the Langmuir Hinshelwood Hougen Watson (LHHW) or microkinetic techniques were effectively conducted for the dry reforming of methane to predict effects of operating temperature, contact time, and feed ratio on conversion of methane, yield of syngas, product selectivity, and ratio of hydrogen to carbon monoxide in produced syngas [24–26]. In this work, a reaction mechanism of the biogas dry reforming is presented. Rate expressions and reaction parameters are formed based on combining of the LHHW~~Langmuir Hinshelwood Hougen Watson (LHHW)~~ and microkinetic methods. The comprehensive kinetic models are applied to gain knowledge about the effect of operating conditions on activity and selectivity of biogas dry reforming.

2. Development of the biogas dry reforming mechanism

A heterogeneous reaction mechanism of biogas dry reforming on a Pt/Rh catalyst is formulated based on the LHHW method. Two possible reactions involved in the mechanism are the CH_4 dry reforming and reverse water-gas shift reactions [27], as shown in R1 and R2, respectively.

R1 $CH_4 + CO_2 \rightleftharpoons 2CO + 2H_2$

R2 $CO_2 + H_2 \rightleftharpoons CO + H_2O$

2.1. CH_4 dry reforming process

To apply the method of LHHW, the catalytic process of CH_4 dry reforming, R1, can be explained in detail as following scheme.

R1.1	$CH_4 + * \rightleftharpoons CH_4*$
R1.2	$CO_2 + * \rightleftharpoons CO_2*$
R1.3	$CH_4* + CO_2* \rightleftharpoons 2CO* + 2H_2*$
R1.4	$2[CO* \rightleftharpoons CO + *]$
R1.5	$2[H_2* \rightleftharpoons H_2 + *]$

The symbol * is vacant sites.
A molecule with * represents the surface species.

For the CH_4 dry reforming proceeding in a relatively high-temperature range, it is reasonably assumed that the surface reaction, R1.3, is the rate determining step (RDS). Then, the LHHW rate expression can be expressed as:

$$R_{DR} = k_{1.3f} K_{CH_4} K_{CO_2} \left(C_{CH_4} C_{CO_2} - \frac{1}{K_{DR}} C_{CO}^2 C_{H_2}^2 \right) \theta_v^2 \quad (1)$$

The values of C_{CH_4}, C_{CO_2}, C_{CO}, and C_{H_2} are the gas phase concentration at catalyst surface of CH_4, CO_2, CO, and H_2, respectively. The term of $k_{1.3f}$ is the rate constant for the forward direction of R1.3 and it is defined in the Arrhenius form as:

$$k_{1.3f} = \frac{A_{1.3}}{\Gamma}\left(\frac{T}{T_o}\right)^{\beta_{1.3}} exp\left(-\frac{E_{1.3}}{RT}\right) \tag{2}$$

The terms of A, Γ, T, T_o, β, E, and R represent for the pre-exponential factor, site density (1.5×10^{15} sites/cm^2 or 2.49×10^{-9} mol/cm^2 [28,29]), absolute temperature, reference temperature (300 K), temperature exponent, activation energy, and universal gas constant (8.314 J/mol·K), respectively. The fraction of vacant sites, θ_v, is given by:

$$\theta_v = \frac{1}{1 + K_{CH_4}C_{CH_4} + K_{CO_2}C_{CO_2} + K_{CO}C_{CO} + K_{H_2}C_{H_2}} \tag{3}$$

K_{CH_4}, K_{CO_2}, K_{CO}, and K_{H_2} are the equilibrium constant for the adsorption process of CH_4, CO_2, CO, and H_2, respectively; and K_{DR} is the equilibrium constant for the overall CH_4 dry reforming, R1.

For the dry reforming of CH_4 taking place at relatively low temperature, it is found that the slowest reaction is switched from the surface reaction, R1.3, to the adsorption of CH_4, R1.1. This means that as soon as the adsorbed CH_4 (CH_4*) is formed, it is rapidly consumed by other reactions. Thus, with the assumption that the CH_4* does not appear on the catalyst surface, the rate expression can be obtained as:

$$R_{DR} = k_{1.1f}\frac{1}{C_{CO_2}}\left(C_{CH_4}C_{CO_2} - \frac{1}{K_{DR}}C_{CO}^2C_{H_2}^2\right)\theta_v \tag{4}$$

The term of $k_{1.1f}$ is the rate constant for the adsorption of CH_4 and it is evaluated by:

$$k_{1.1f} = \frac{s_{CH_4}}{\Gamma}\sqrt{\frac{RT}{2\pi M}}\left(\frac{T}{T_o}\right)^{\beta_{1.1}} exp\left(-\frac{E_{1.1}}{RT}\right) \tag{5}$$

The term s_{CH4} stands for the sticking coefficient of methane adsorbing on the catalyst surface and M is the molecular weight of methane. The site vacancies are calculated by:

$$\theta_v = \frac{1}{1 + K_{CO_2}C_{CO_2} + K_{CO}C_{CO} + K_{H_2}C_{H_2}} \tag{6}$$

2.2. Reverse water-gas shift process

The reverse water-gas shift process, R2, which takes place simultaneously with the CH_4 dry reforming, R1, can be detailed as:

R2.1	$H_2 + 2^* \rightleftharpoons H^* + H^*$
R2.2	$CO_2 + H^* \rightleftharpoons CO + OH^*$
R2.3	$OH^* + H^* \rightleftharpoons H_2O^* + *$
R2.4	$H_2O^* \rightleftharpoons H_2O + *$

By obtaining the activation of CO_2, R2.2, as the RDS, the LHHW rate expression is formulated as:

$$R_{RWGS} = k_{2.2f}\sqrt{K_{2.1}}\left(C_{CO_2}C_{H_2} - \frac{1}{K_{RWGS}}C_{CO}C_{H_2O}\right)\theta_v \quad (7)$$

The rate constant for the forward direction of R2.2, $k_{2.2f}$, is obtained as:

$$k_{2.2f} = \frac{A_{2.2}}{\Gamma}\left(\frac{T}{T_o}\right)^{\beta_{2.2}} exp\left(-\frac{E_{2.2}}{RT}\right) \quad (8)$$

The unoccupied surface sites are estimated by:

$$\theta_v = \frac{1}{\sqrt{C_{H_2}} + \sqrt{K_{2.1}}C_{H_2} + K_{H_2O}C_{H_2O}\sqrt{C_{H_2}} + \frac{1}{\sqrt{K_{2.1}}K_{2.3}}K_{H_2O}C_{H_2O}} \quad (9)$$

As $K_{2.1}$ and $K_{2.3}$ are the equilibrium constant of the reaction R2.1 and R2.3, respectively; and K_{RWGS} is the equilibrium constant of the gas-phase reverse water-gas shift process, R2.

3. Determination of reaction parameters

3.1. Activation energies

Three activation energies for: i) the dry reforming as the surface reaction is the RDS; ii) the dry reforming as the adsorption of CH_4 is the RDS; and iii) the reverse water-gas shift reaction are calculated by applying the microkinetic approach [30] and the theory of unity bond index-quadratic exponential potential (UBI-QEP) [31–33]. Recently, the UBI-QEP theory was successfully employed with the novel method of density functional theory (DFT) to explain at molecular level of catalytic reactions of methane over platinum and rhodium surfaces [34].

According to the microkinetic approach, mechanistic details of CH_4 dry reforming, heats of reaction, and activation energies for each step are given in Table 1. The mechanism consists of activated adsorptions of reactants (e.g., reactions DR1-DR3), surface reactions (DR4-DR7), and desorption of products (DR8 and DR9). As already mentioned, at relatively high temperature the surface reaction kinetically controls the overall rate of CH_4 dry reforming process. This assumption is complied with previous publications which indicate that the decompositions of adsorbed CH_4 are the RDS [27,28,35,36]. Thus, the activation energy for this situation is selected from the highest value of the surface reactions (DR4-DR7) in the forward direction. Therefore, the value of 32.12 kcal/mol (from thermal cracking of CH* [36], DR6) is chosen to represent the activation energy of the CH_4 dry reforming process at relatively high temperature. At relatively low temperature, it is found that the RDS is changed from the surface reaction to the dissociative adsorption of CH_4. So, the value of forward-direction activation energy, 19.82 kcal/mol, is picked to represent the activation energy of the dry reforming process at relatively low temperature. Moreover, the activation of the co-reactant, CO_2, with surface hydrogen (H*) to form highly active species OH* was proposed as the crucial step whereas the directly dissociative adsorption of CO_2 to produce adsorbed CO was negligible [27,28,36]. Therefore, the highest value of 26.95 kcal/mol shown in Table 2 is selected as the activation energy for the reverse water-gas shift reaction.

Table 1

Detailed reaction mechanism of CH_4 dry reforming process.

	Reactions	Δh_R [a] (kcal/mol)	E_{for} [b] (kcal/mol)	E_{rev} [c] (kcal/mol)
DR1	$CH_4 + * \rightleftharpoons CH_4*$	-19.22	0.00	19.22
DR2	$CH_4* + * \rightleftharpoons CH_3* + H*$	11.92	19.82	7.90
DR3	$CO_2 + H* \rightleftharpoons CO + OH*$	26.95	26.95	0.00
DR4	$CH_3* + * \rightleftharpoons CH_2* + H*$	2.80	20.25	17.45

DR5	$CH_2^* + * \rightleftharpoons CH^* + H^*$	-29.80	7.70	37.50
DR6	$CH^* + * \rightleftharpoons C^* + H^*$	19.10	32.12	13.02
DR7	$C^* + OH^* \rightleftharpoons CO^* + H^*$	-36.41	3.71	40.12
DR8	$H^* + H^* \rightleftharpoons H_2 + 2^*$	20.85	20.85	0.00
DR9	$CO^* \rightleftharpoons CO + *$	42.00	42.00	0.00

[a] Heat of reaction
[b] Activation energy of forward reaction
[c] Activation energy of reverse reaction

Table 2

Detailed reaction mechanism of reverse water-gas shift process.

	Reactions	Δh_R (kcal/mol)	E_{for} (kcal/mol)	E_{rev} (kcal/mol)
RWGS1	$H_2 + 2^* \rightleftharpoons H^* + H^*$	-20.85	0.00	20.85
RWGS2	$CO_2 + H^* \rightleftharpoons CO + OH^*$	26.95	26.95	0.00
RWGS3	$OH^* + H^* \rightleftharpoons H_2O^* + *$	-6.51	12.05	18.56
RWGS4	$H_2O^* \rightleftharpoons H_2O + *$	10.20	10.20	0.00

3.2. Equilibrium constants

An equilibrium constant of gas molecule i, K_i, adsorbing on a surface catalyst can be computed by using the knowledge about transition state theory (TST) [37].

$$K_i = exp\left(\frac{\Delta s^{0\ddagger}}{R}\right) exp\left(-\frac{Q_i}{RT}\right) \quad (10)$$

Heats of adsorption of gas-phase species i, Q_i, used in this work are calculated via the UBI-QEP theory and listed in Table 3.

Table 3

Heat of adsorption on Pt catalyst.

Species	Heat of adsorption, Q (kcal/mol)

CH_4	19.22
CH_3	49.80
CH_2	95.00
CH	163.30
C	162.60
H	62.50
H_2	6.69
H_2O	10.20
OH	60.00
CO	42.00
CO_2	4.50

The standard entropy change, $\Delta s^{0\ddagger}$, during an adsorption process of a gas molecule is expressed as:

$$\Delta s^{0\ddagger} = R\left[ln\left(\frac{\frac{h}{k_B T}}{(2\pi m k_B T)^{1/2}}\left(\frac{A}{N}\right)P^0\right) - \frac{1}{2}\right] \quad (11)$$

where h, k_B, m, A/N, and P^0 stand for Planck constant, Boltzmann constant, mass per molecule, area occupied per adsorbed molecule, and standard pressure, respectively. Variation in temperatures of equilibrium constants is estimated by application of the van't Hoff equation [38].

4. Simulation

The simulation is set up following experiments presented in our previous publication [14]. The monolithic catalyst size was 20 mm in diameter and 75 mm in length. The reforming catalyst was made from a high-cell density cordierite (900 cells per square inch) which was coated with 2% Pt and 1% Rh (by mass) dispersed on 30% (by mass) ceria-zirconia (3:1 mol ratio) and 70% γ-Al_2O_3. In the simulation part, a single channel is selected from the monolithic

catalyst to study computationally. The channel is reasonably assumed to be an axisymmetric cylinder with radius of 0.2663 mm. Physical and chemical phenomena taking place inside the channel are examined by using the commercial software ANSYS FLUENT 14.

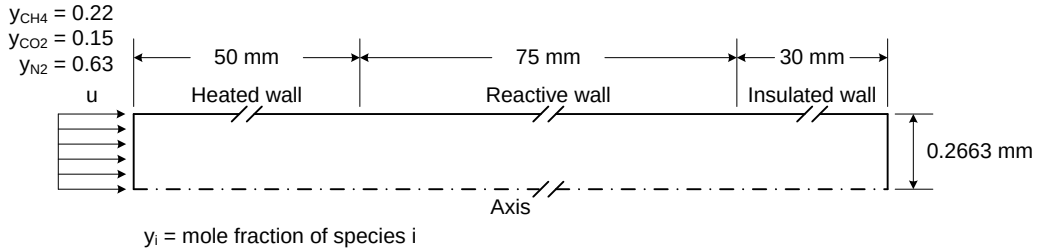

Fig. 1. Computational domain.

The computational domain is separated into three different zones as illustrated in Fig. 1. In the first zone, wall temperature is specified to be equal to the operating temperature; so the temperature of reactants is increased from the ambient to required value. No chemical reaction occurs in the heating up zone. The second zone is where the surface chemical reactions occur causing for depletion of reactants and formation of products. Due to highly endothermic process of CH_4 dry reforming, external energy provided in this zone is necessary. The heat required to be supplied in order to proceed the dry reforming system, $\dot{Q}_{in}$, is calculated from:

$$\dot{Q}_{in} = \eta_{CH_4} \dot{n}_{CH_4} \Delta h^0_{R,T} \tag{12}$$

Conversions of CH_4, η_{CH_4}, are taken from our experiments [14]. Molar flow rate of CH_4, $\dot{n}_{CH_4}$, is obtained from:

$$\dot{n}_{CH_4} = \frac{P_{in} \dot{V}_{CH_4}}{RT} \tag{13}$$

The inlet pressure, P_{in}, of 170000 Pa is used for all simulations imitating the value that was used in our previous experiments [14]. The enthalpy change, $\Delta h^0_{R,T}$, during the dry reforming process (R1) is estimated from [38]:

$$\Delta h^0_{R,T} = \Delta h^0_{R,298} + \frac{1}{\alpha_{CH_4}} \left[\int_{298}^{T} \left(\sum_{products} \alpha_i C_P - \sum_{reactants} \alpha_i C_P \right) dT \right] \tag{14}$$

$\Delta h^0_{R,298}$, α_i, and C_P are standard heat of reaction, stoichiometric coefficient of species i (e.g., CH_4, CO_2, CO, and H_2), and heat capacity, respectively. Supplied heat flux in different operating conditions is listed in Table 4. The last zone is presented in order to avoid problems generated from the back pressure at the end of the computational domain. Both supplied heat and chemical reactions are omitted in the last zone. Inlet mole fractions of CH_4 and CO_2 are, respectively, 0.22 and 0.15 to represent the biogas consisting of 60%vol of CH_4 and 40%vol of CO_2. Nitrogen with mole fraction of 0.63 is used as the balance gas. Inlet velocities are 0.8685 and 1.4475 m/s for the gas hourly space velocity (GHSV) of 16500 and 27500 h^{-1}, respectively. Note, to avoid the divide by zero problem (e.g., Eq (9)), the mole fraction of products is specified as a very small value at the initial condition.

Table 4

Supplied heat for dry reforming of CH_4.

Operating temperature (°C)	Heat flux (W/m^2)
GHSV 16500 h^{-1}	
660	1333
770	1525
870	1697
950	1874
GHSV 27500 h^{-1}	
625	2325
730	2509
840	2755
910	2907

5. Optimisation

The advantage of LHHW over microkinetic approach is that numbers of chemical reaction are fairly low. So, a sensitivity analysis (SA) is unnecessary to identify important reactions and parameters. In this work, six active parameters (one sticking coefficient, two pre-exponential factors, and three temperature exponents) are needed to be optimised. To avoid the difference in value by many orders of magnitude, the active parameters are scaled to a value which is in the range between -1 and 1. The scaled parameters, *X*, (called factorial variables) are defined by the following relation [39].

$$X = \frac{ln\left(\frac{A^2}{A_{min}A_{max}}\right)}{ln\left(\frac{A_{max}}{A_{min}}\right)} \quad (15)$$

Conversion of CH_4 and productions of H_2 and CO are selected as model responses. A relation of the model responses with several values of factorial variable is systematically constructed and formulated as a second order polynomial. Linear regression analysis is then applied to calculate the values of the factorial variables in order to minimise the error between simulations and experiments [39]. The optimised values including activation energies are summarised in Table 5.

Table 5

Optimised kinetic parameters for the biogas dry reforming and water-gas shift on the platinum-rhodium alumina catalyst.

$A_{1.3}$	(s^{-1})	3.5×10^{7}
$\beta_{1.3}$	(-)	2.0
$E_{1.3}$	(kcal/mol)	32.12
s_{CH4}	(-)	9.4528×10^{-6}
$\beta_{1.1}$	(-)	1.5483
$E_{1.1}$	(kcal/mol)	19.82
$A_{2.2}$	(s^{-1})	0.01

$\beta_{2.2}$	(-)	−1.8
$E_{2.2}$	(kcal/mol)	26.95

6. Results and discussions

6.1. Validation

The validations between model predictions and experimental data are displayed in Figs. 2-6. Note: To follow the results previously published [14], the reactant and product distributions of all conditions are normalised by nitrogen content. The conversions of CH_4 and CO_2, and yield of CO and H_2 are defined as:

$$CH_4\ conversion\ (\%) = \frac{[CH_4]_{inlet} - [CH_4]_{outlet}}{[CH_4]_{inlet}} \times 100 \quad (16)$$

$$CO_2\ conversion\ (\%) = \frac{[CO_2]_{inlet} - [CO_2]_{outlet}}{[CO_2]_{inlet}} \times 100 \quad (17)$$

$$CO\ yield\ (\%) = \frac{[CO]/2}{[CH_4]_{inlet}} \times 100 \quad (18)$$

$$H_2\ yield\ (\%) = \frac{[H_2]/2}{[CH_4]_{inlet}} \times 100 \quad (19)$$

With optimised parameters given in Table 5, comparisons of modelling results with measured data are presented in Fig. 2. The linearity between simulation and experiment, R^2, for all cases is greater than 0.9 and the predicted values are within the margin of ±10% deviation except for CO_2 which simulation predicts lower CO_2 concentration comparing with experiment.

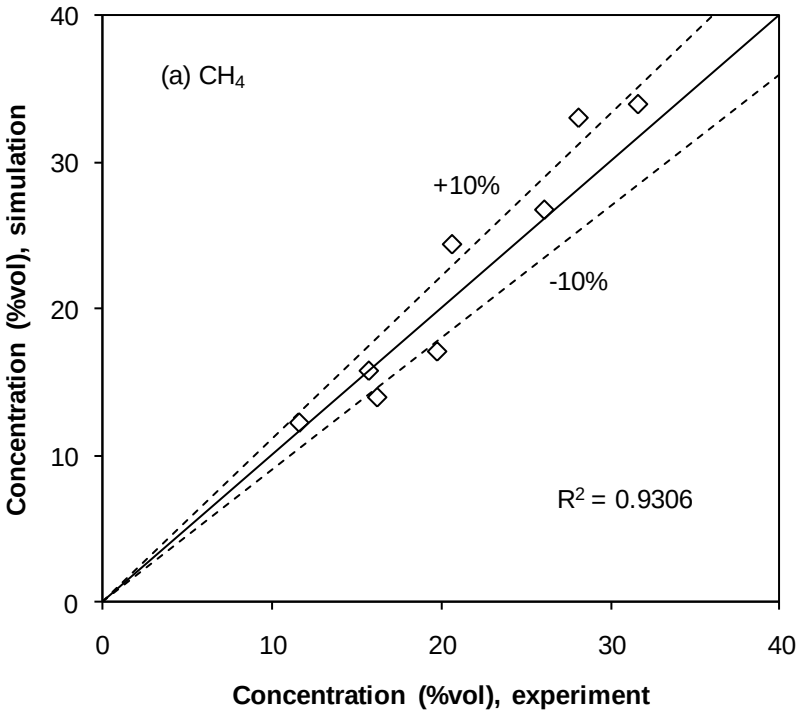
(a) CH_4
+10%
-10%
R^2 = 0.9306
Concentration (%vol), simulation
Concentration (%vol), experiment
0
10
20
30
40

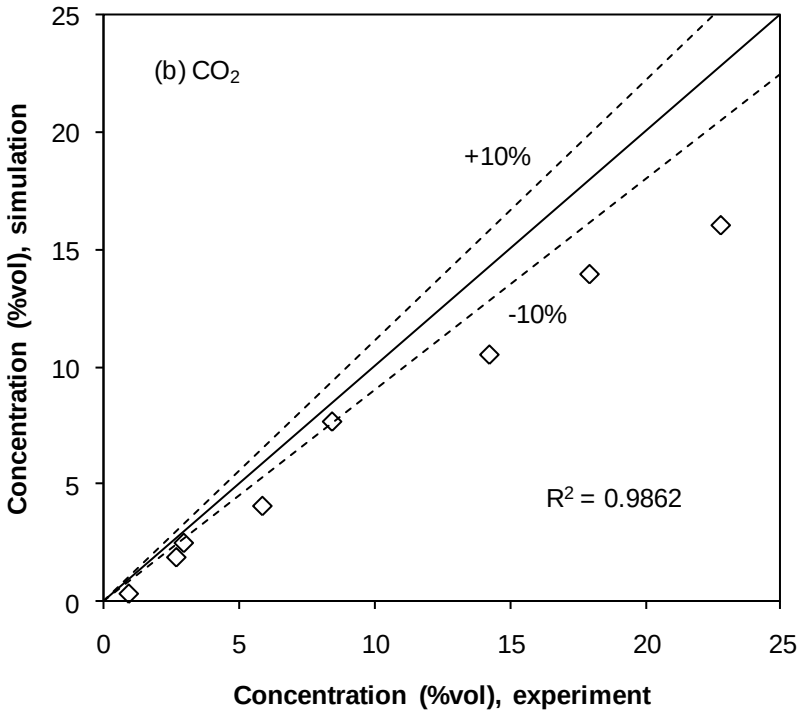
(b) CO_2
+10%
-10%
R^2 = 0.9862
Concentration (%vol), simulation
Concentration (%vol), experiment
0
5
10
15
20
25

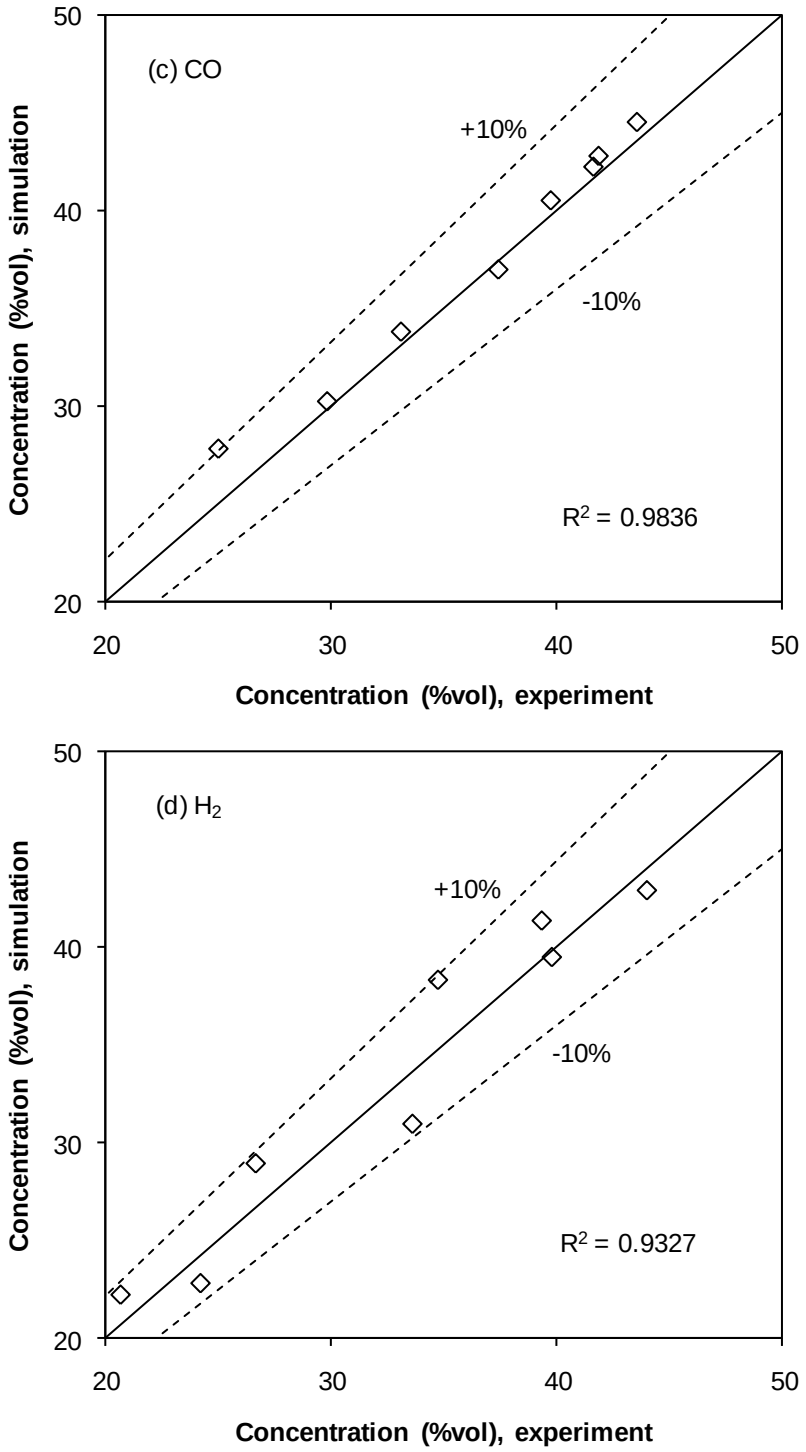

Fig. 2. Parity plots of biogas dry reforming between simulation and experimental data.

Effect of reactor temperature and space velocity on outlet concentration of reactants (e.g., CH_4 and CO_2) and products (e.g., CO and H_2) is illustrated in Fig. 3. Since the dry reforming of CH_4 is the highly endothermic process, the conversion of reactants and creation of products relate

primarily to operating temperature (supplied heat). In contrast, the space velocity has small effect on the reforming process. Results from model show good agreement with measured data.

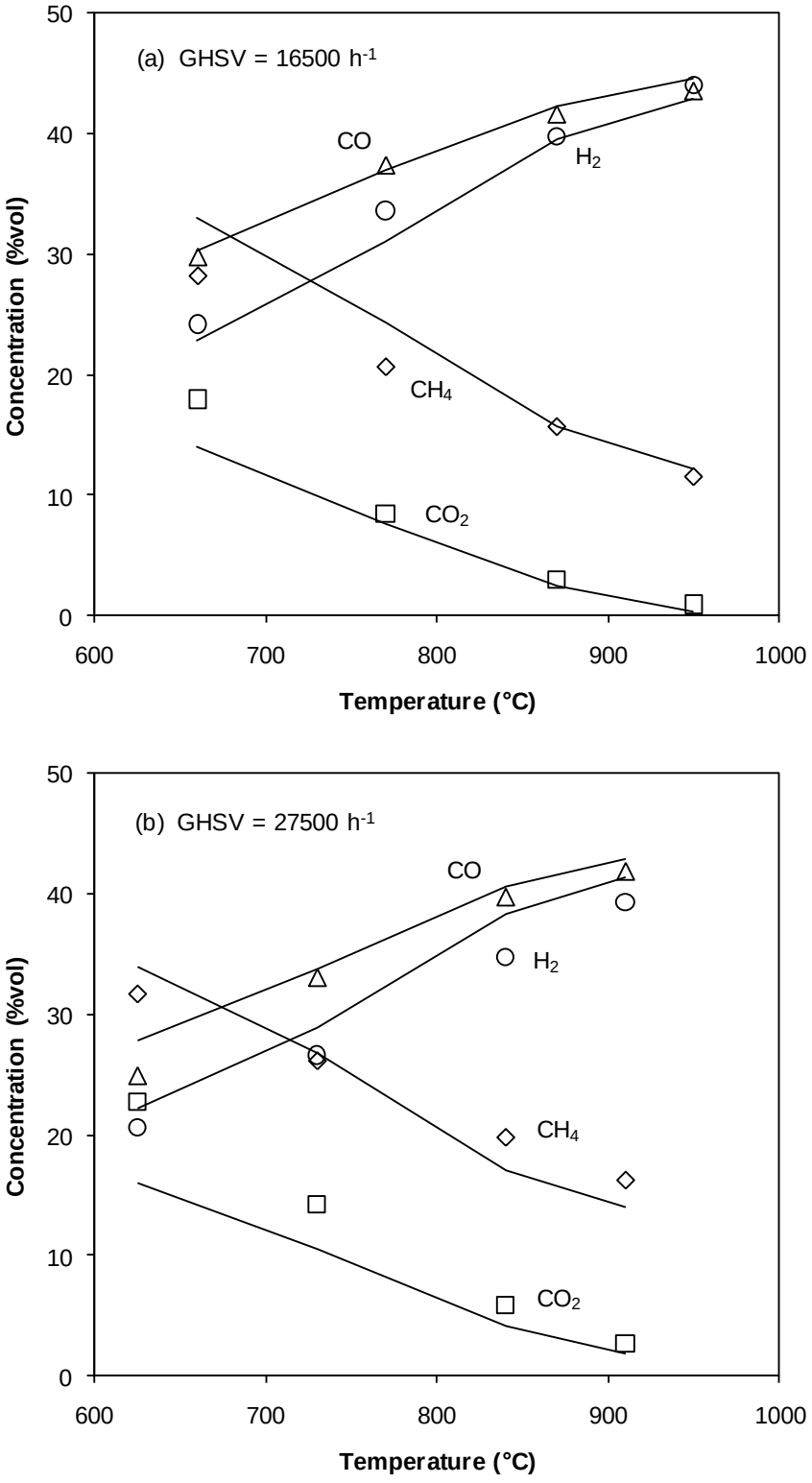

Fig. 3. Outlet concentrations of reactants and products at different operating temperatures and space velocities. (Solid lines: simulation. Symbols: experimental data [14]).

The conversion of reactants into products is illustrated in Fig. 4. The model gives higher conversion than that of experiment for both CH_4 and CO_2. The conversion of CO_2 is larger than that of CH_4. The higher conversion of CO_2 was also found in the literature [27] at CH_4:CO_2 of 1:1. However, when the concentration of CO_2 was increased, for instance CH_4:CO_2 of 1:2 and 1:4, the conversion of CH_4 was larger than CO_2. The conversion at equilibrium state is estimated by using the chemical equilibrium calculation freeware, Gaseq. It indicates the maximum conversion that can be reached at a specific condition (e.g., operating temperature and starting composition of reactants). The figure gives information that at CH_4:CO_2:N_2 of 0.22:0.15:0.63 (actual mole fraction at inlet) or CH_4:CO_2 of 60:40 (percentage after normalised by nitrogen content), the possible conversions of CH_4 and CO_2 are 80 and 100%, respectively, which occur at high temperatures. The conversions obtained from both simulation and experiment approaches the equilibrium values at high temperatures. Nevertheless, at relatively low temperatures, the conversions are much lower than that evaluated from the equilibrium calculation. This suggests that at relatively low temperatures the biogas dry reforming carries out far from the equilibrium state.

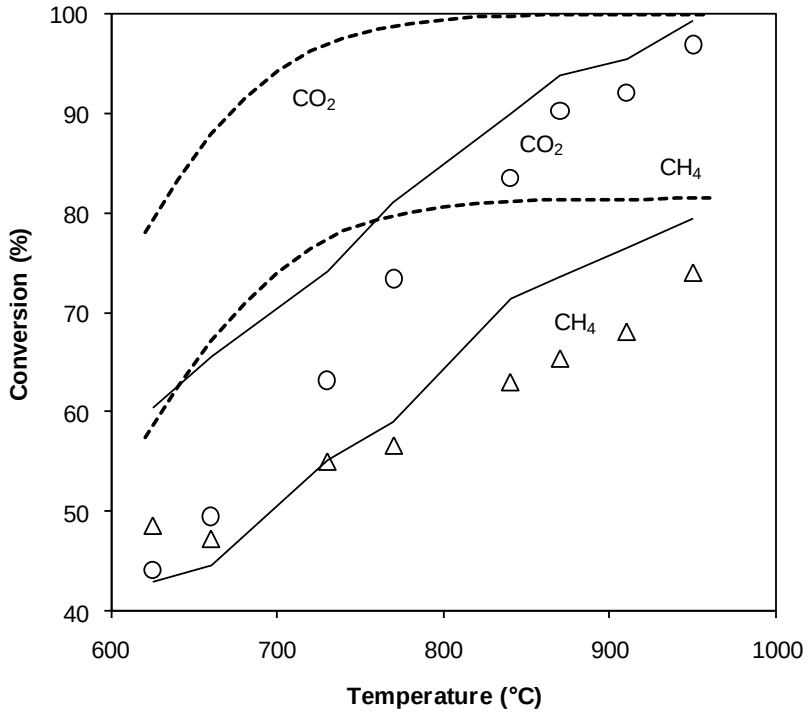

Fig. 4. Conversions of CH_4 and CO_2 at different operating temperatures (Solid lines: simulation. Symbols: experimental data [14]. Dash lines: equilibrium calculation).

Fig. 5 compares yields of CO and H_2 obtained from experiment, modelling, and equilibrium calculation. The yields estimated from the equilibrium calculation represents the maximum yield that can be achieved at a temperature. The figure indicates that the maximum yield is around 37% and can be found in relatively high temperatures. The model shows that the yields of CO and H_2 are close to the values taken from experiments.

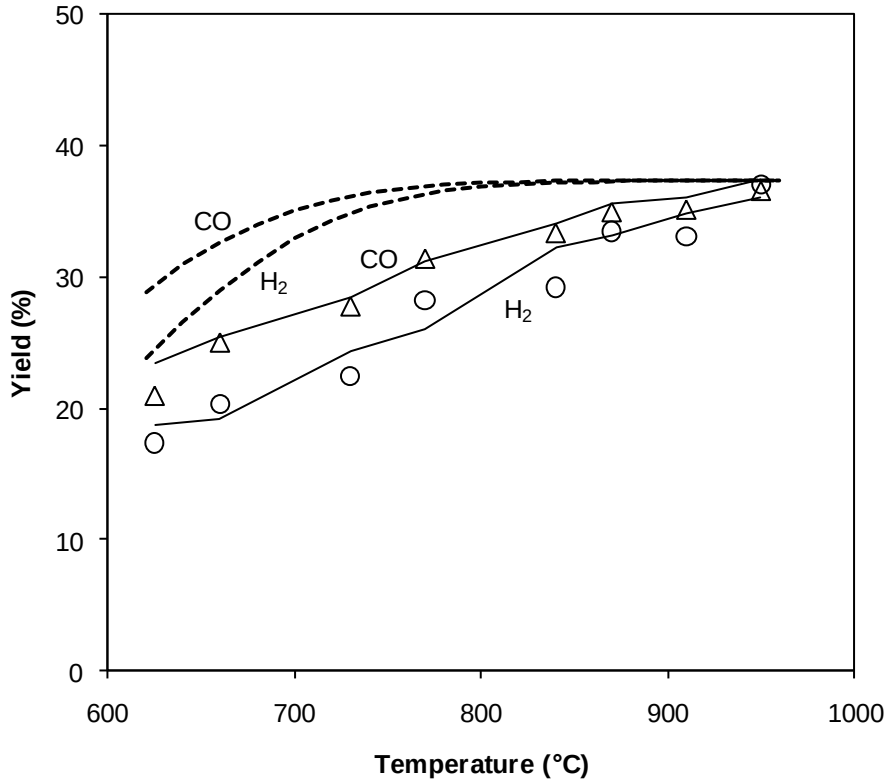

Fig. 5. Yields of CO and H_2 at different operating temperatures (Solid lines: simulation. Symbols: experimental data [14]. Dash lines: equilibrium calculation).

The effect of reverse water gas shift is illustrated in Fig. 6. Two moles of both CO and H_2 are expected to generate from one mole of CH_4 and CO_2 according to the dry reforming pathway, R1. However, the existence of the reverse water gas shift consumes the produced H_2 with CO_2 to create CO which results that the ratio of H_2 to CO is smaller than unity for every operating condition. The H_2 to CO ratio tends to increase as operating temperatures are risen. This

suggests that at relatively high temperatures, dry reforming reaction is more favourable than the reverse water gas shift.

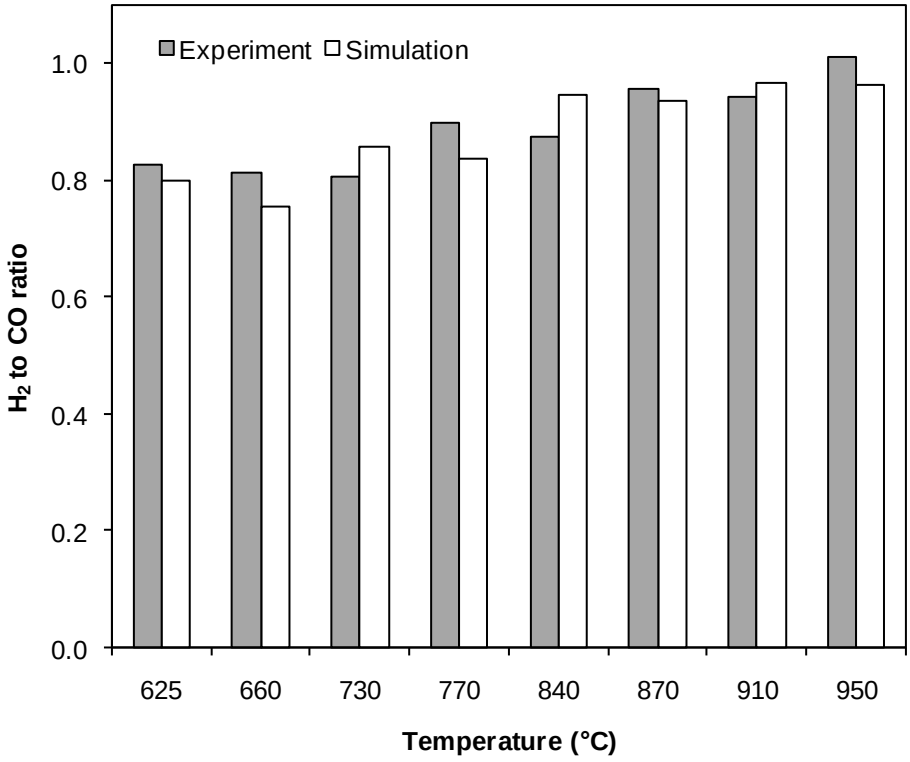

Fig. 6. Comparisons between model predictions and experimental data for the H_2 to CO ratio at various operating temperatures.

6.2. Simulations of biogas dry reforming

In this section, effects on the biogas dry reforming activities (e.g., gas composition, temperature profile inside catalyst, CH_4 and CO_2 conversions, CO and H_2 yields, and H_2 to CO ratio) of operating conditions (for instant, inlet concentrations of CH_4 and CO_2, inlet temperature, and supplied heat) are predicted without any modification of reaction parameters.

To produce hydrogen from biogas by using the exothermic partial oxidation process, a too high temperature hot spot is avoided. The dry reforming is expected not only to provide more hydrogen production but also to reduce the hot spot temperature resulting from the partial oxidation. With attention to use the endothermic dry reforming to decrease the hot spot temperature during the exothermic partial oxidation which generally proceeds at around 800-

1000 °C, the simulation is performed under high inlet temperatures with and without heat supplied at the catalyst wall.

6.2.1. The effect of inlet temperature on CH_4 dry reforming activity

The effects of inlet temperature and inlet CH_4 to CO_2 ratio on reactant and product concentration at catalyst outlet are shown in Fig. 7. Slow drop of CH_4 and CO_2 (Fig. 7(a) and (b)), as the inlet temperature increases indicates that consumption of reactants increases gradually with the temperature. As the inlet CH_4 to CO_2 ratio increases (with constant CO_2 composition at 15%vol), the improved availability of CH_4 enhanced the dry reforming reaction that consumed additional CO_2 (Fig. 7(b)). In contrast, with limited CO_2 supply, unreacted CH_4 grows quickly resulting in an increase of outlet CH_4 concentration at high CH_4 to CO_2 ratio (Fig. 7(a)). Fig. 7(c) and (d) suggests that CO and H_2 production was improved steadily, with an increase in the inlet temperature. Interestingly, as the inlet CH_4 to CO_2 ratio increases, CO and H_2 show a drop in concentration. Both components concentration should have been increased as more CO_2 was conversed (Fig. 7(b)). However, both gases CO and H_2 compositions are calculated through the concentration of each individual component divided by total mixture (not including N_2). As already mentioned, addition of CH_4 results in larger divider and makes lower relative CO and H_2 concentration.

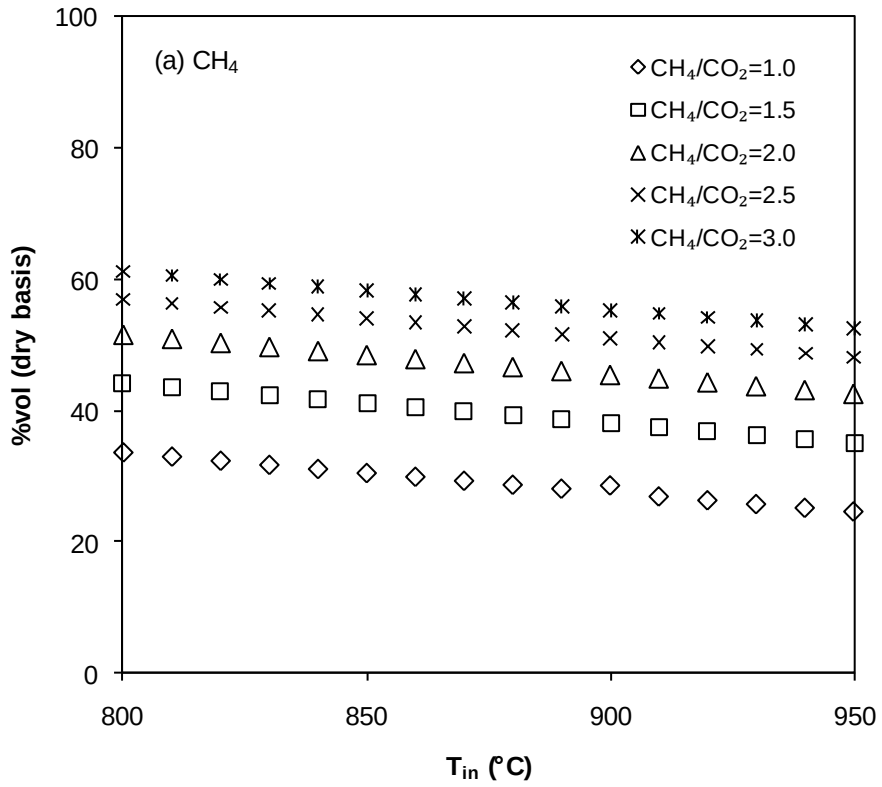
(a) CH4
CH4/CO2=1.0
CH4/CO2=1.5
CH4/CO2=2.0
CH4/CO2=2.5
CH4/CO2=3.0
%vol (dry basis)
Tin (°C)
0
20
40
60
80
100
800
850
900
950

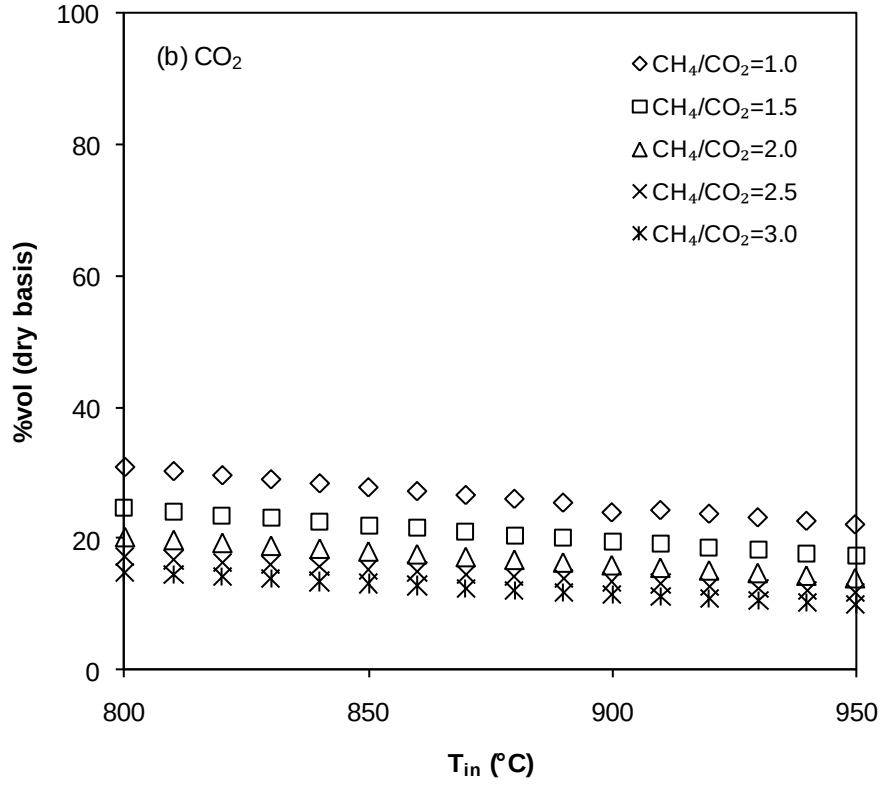
(b) CO2
CH4/CO2=1.0
CH4/CO2=1.5
CH4/CO2=2.0
CH4/CO2=2.5
CH4/CO2=3.0
%vol (dry basis)
Tin (°C)
0
20
40
60
80
100
800
850
900
950

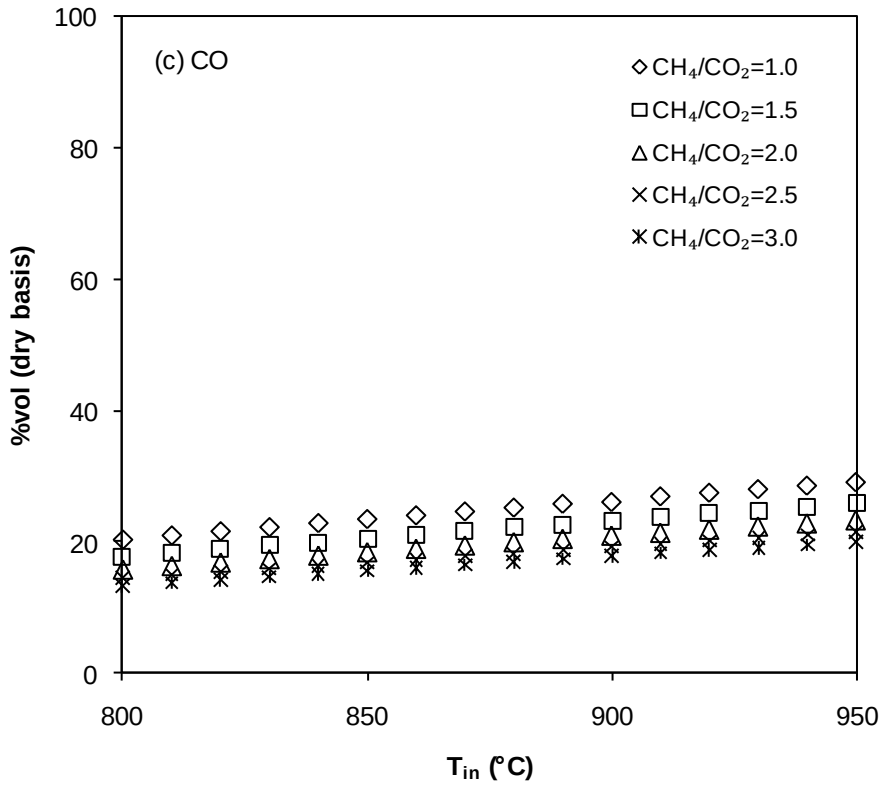

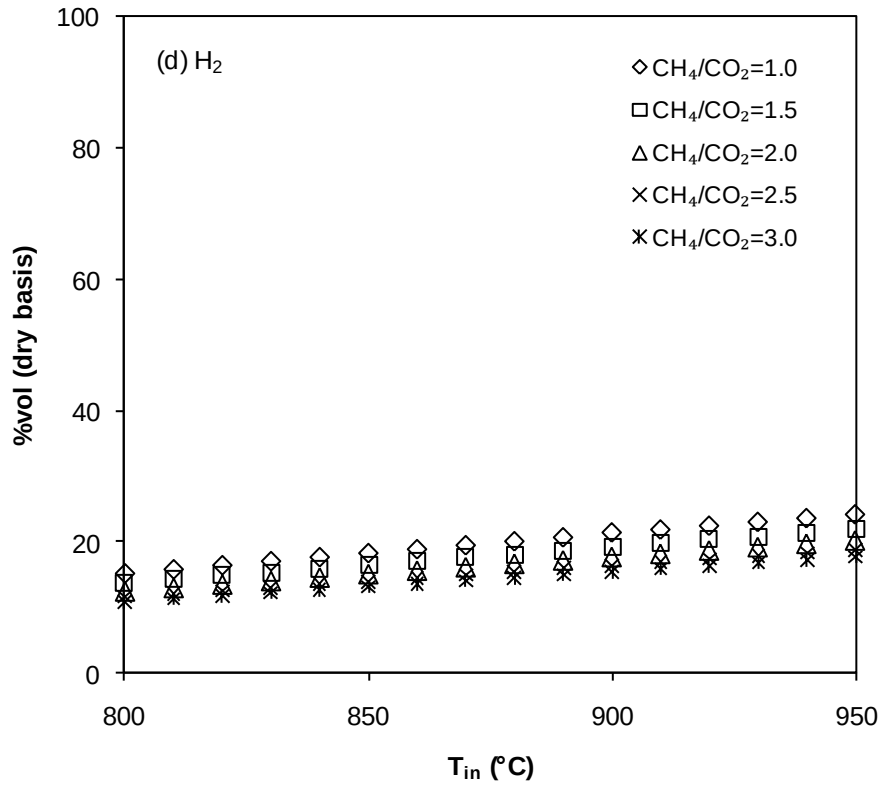

Fig. 7. Model prediction of reactant and product concentrations as a function of inlet temperature at different CH_4 to CO_2 ratios. Inlet conditions: constant CO_2 composition of 15 %vol; GHSV of 27500 h^{-1}; no supplied heat on reactive wall.

Axial and radial velocities and pressure distribution are calculated from the Navier-Stokes equation. Without the assumption about the CH_4 dry reforming taking place under isothermal condition, the temperature profiles inside the channel of catalyst, as shown in Fig. 8, can be obtained by solving the energy equation. The substantial drop of wall and axial temperatures suggests that the endothermic CH_4 dry reforming suddenly starts at the catalyst entrance. Both temperatures approach the same value at around 25 mm of catalyst length for all inlet temperatures. This length indicates the end of chemical activity and is independent on the inlet temperature. Thus, just one third of the catalyst is active and on the catalyst surface beyond this point, there is no existence of dry reforming reaction.

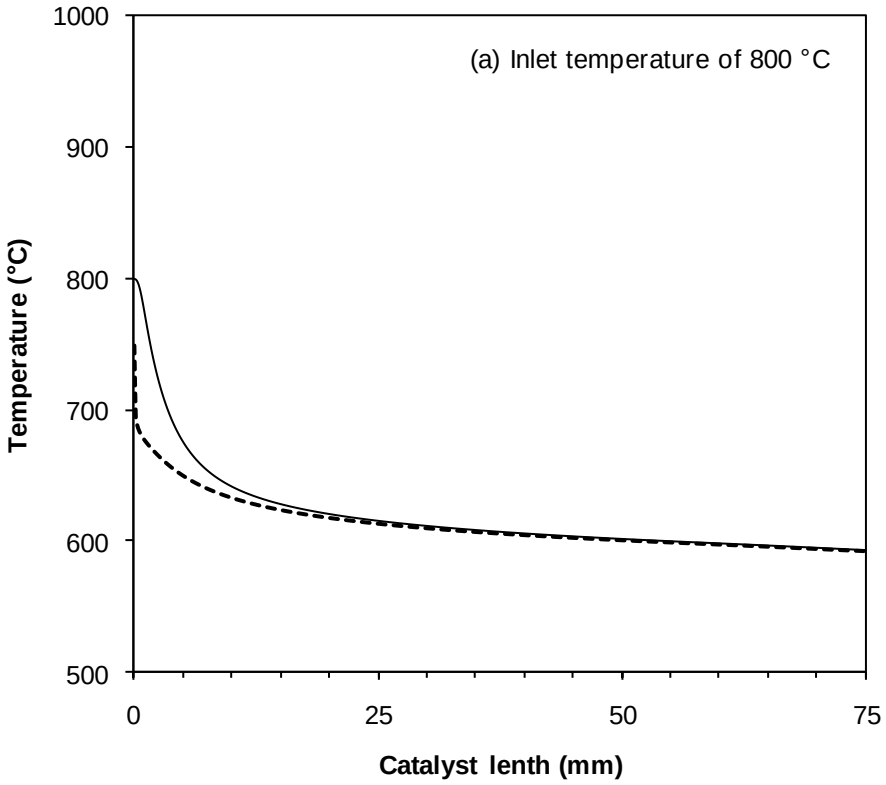

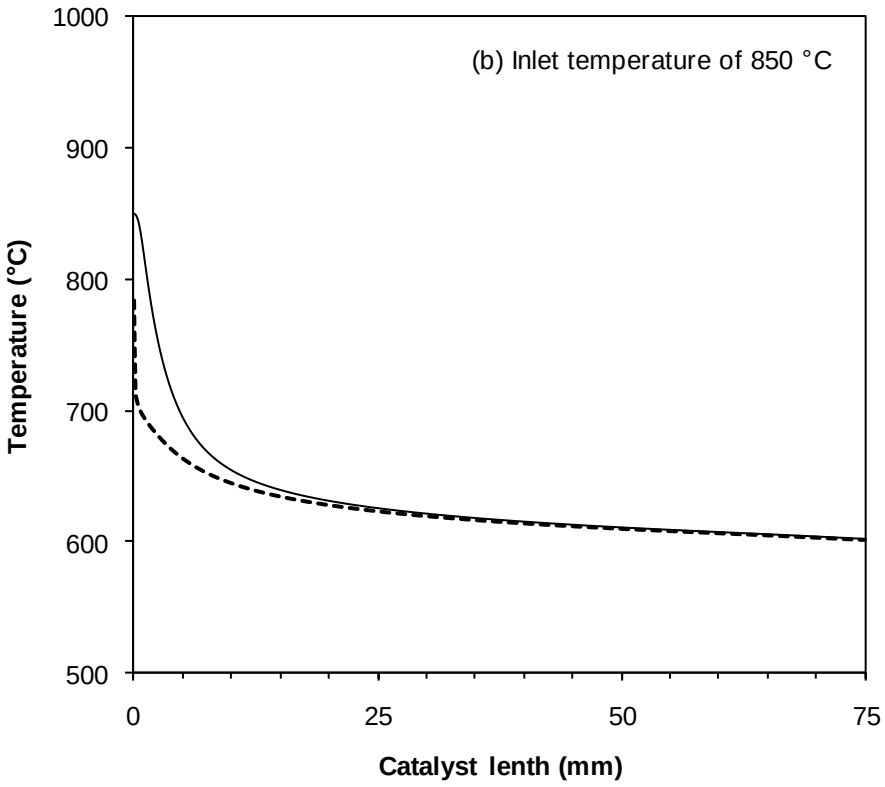
(b) Inlet temperature of 850 °C
1000
900
800
700
600
500
Temperature (°C)
0
25
50
75
Catalyst lenth (mm)

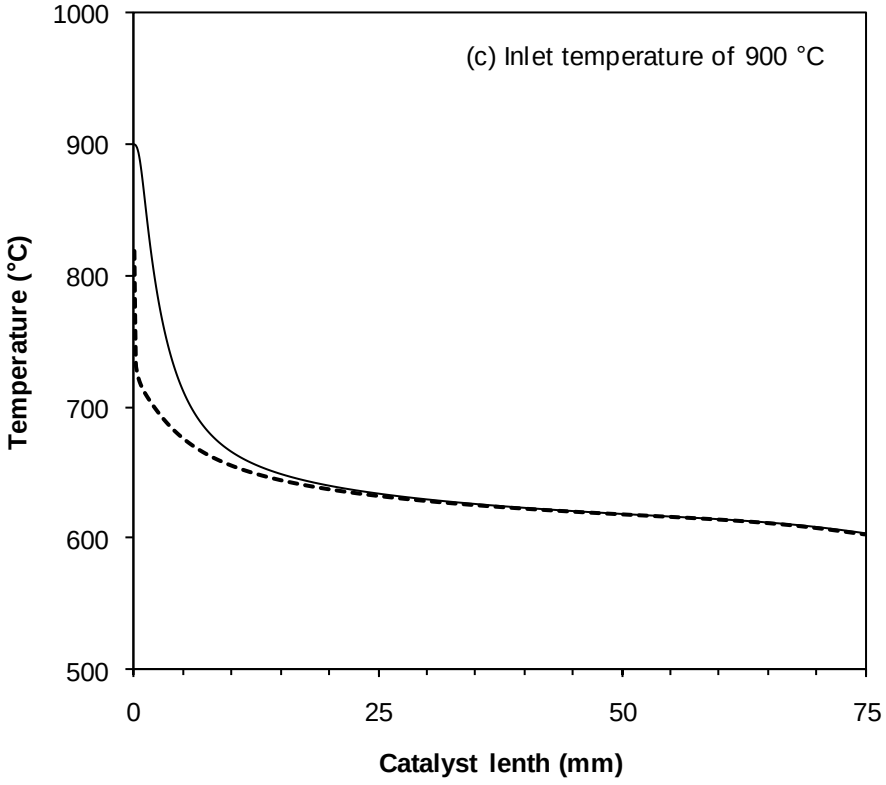
(c) Inlet temperature of 900 °C
1000
900
800
700
600
500
Temperature (°C)
0
25
50
75
Catalyst lenth (mm)

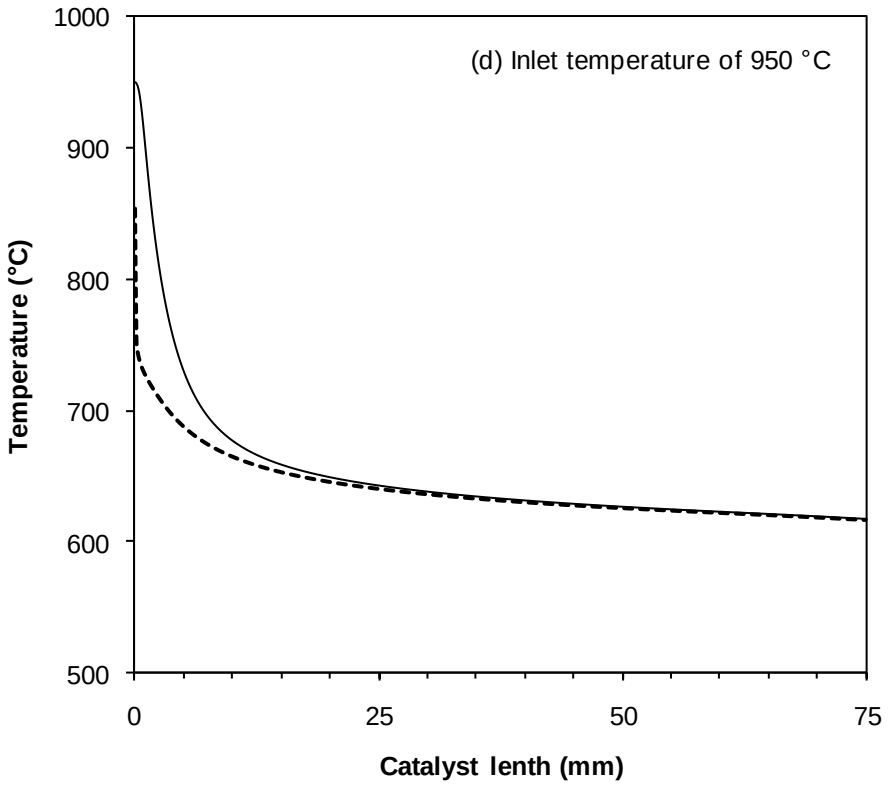

Fig. 8. Temperature profiles inside the catalyst at different inlet temperatures. Inlet conditions: CO_2 composition of 15 %vol; CH_4 to CO_2 ratio of 1; GHSV of 27500 h^{-1}; no supplied heat on reactive wall. (Solid line: axial temperature. Dash lines: wall temperature.)

Comparison of difference in axial and wall temperatures is shown in Fig. 9. Higher inlet temperature gives higher temperature difference which states higher rate of chemical reaction occurring according to Arrhenius law. Interestingly, the highest activity of each inlet temperature (top of the hills) takes place at the same position (0.5 mm).

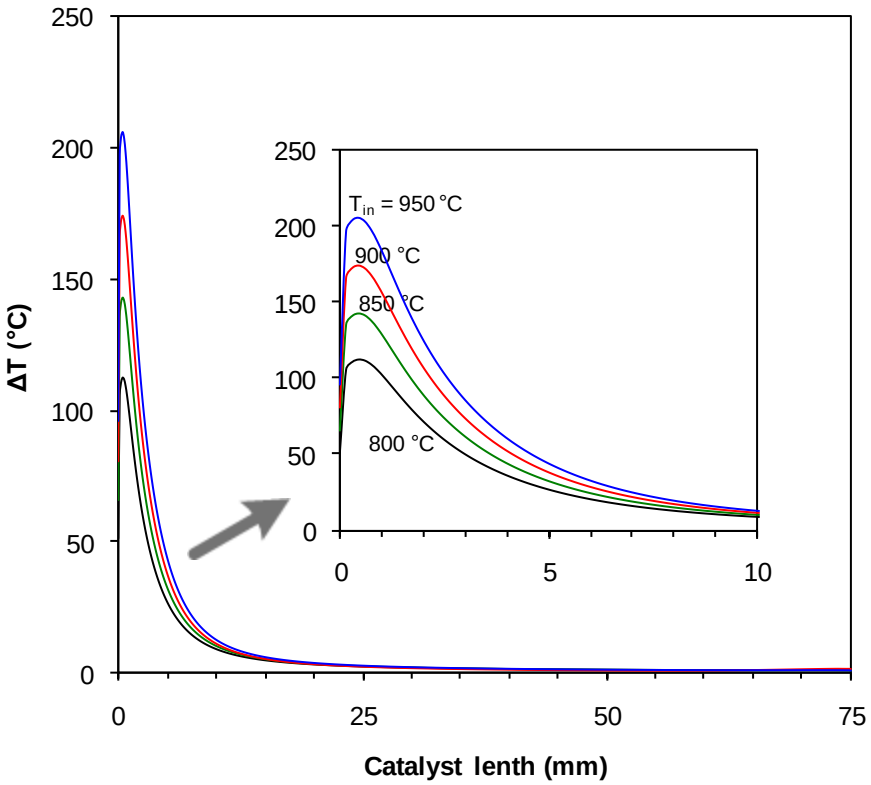

Fig. 9. Difference between axial and wall temperatures at various inlet temperature. Inlet conditions are given in Fig. 8.

The activity of highly endothermic CH_4 dry reforming occurs at high temperatures, potentially near the catalyst durability limits. As expected, conversions of CH_4 and CO_2 vary proportionally with the temperature. Since no heat is supplied to the catalyst wall, conversions of CH_4 and CO_2 were limited to around 40-50%. Decrease of CH_4 conversion, Fig. 10(a), as CH_4 to CO_2 ratio raised is noticed due to remaining of excess CH_4, as already stated. Conversions of CO_2, Fig. 10(b), are almost independent of CH_4 to CO_2 ratio due to its constant composition (15 %vol) at inlet. Their conversions are higher than that of CH_4 because it is consumed via both dry reforming with CH_4 and reverse water–gas shift with H_2.

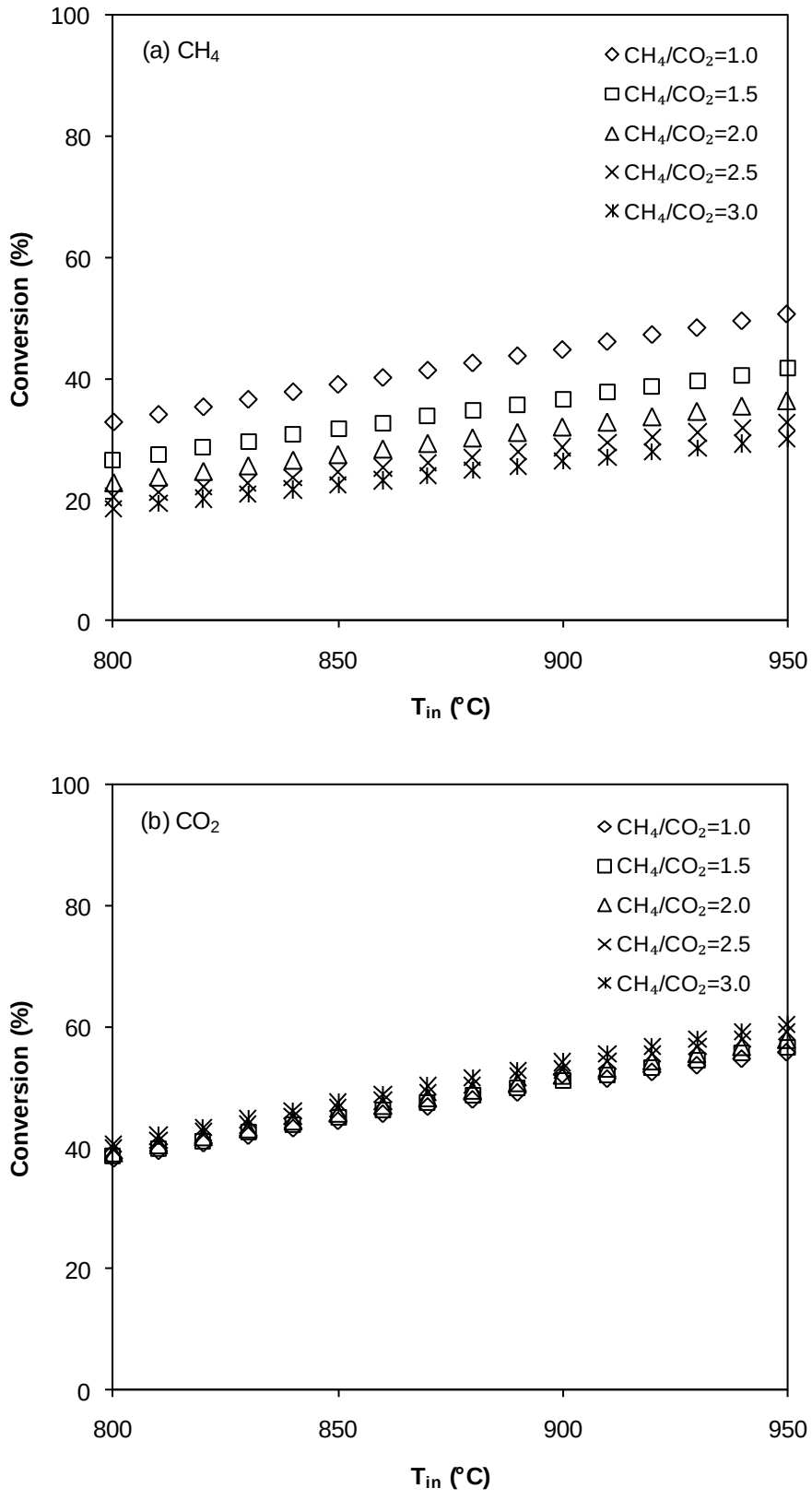

Fig. 10. Prediction of CH_4 and CO_2 conversions as a function of inlet temperature at different CH_4 to CO_2 ratios. Inlet conditions are given in Fig. 7.

Yields of CO and H_2 as a function of inlet temperature and inlet CH_4 to CO_2 ratio are presented in Fig. 11. The product yields rise slowly with inlet temperature. The drops in product yield with increases of CH_4 to CO_2 ratio are resulted from the declines of CH_4 conversion, Fig. 10 (a).

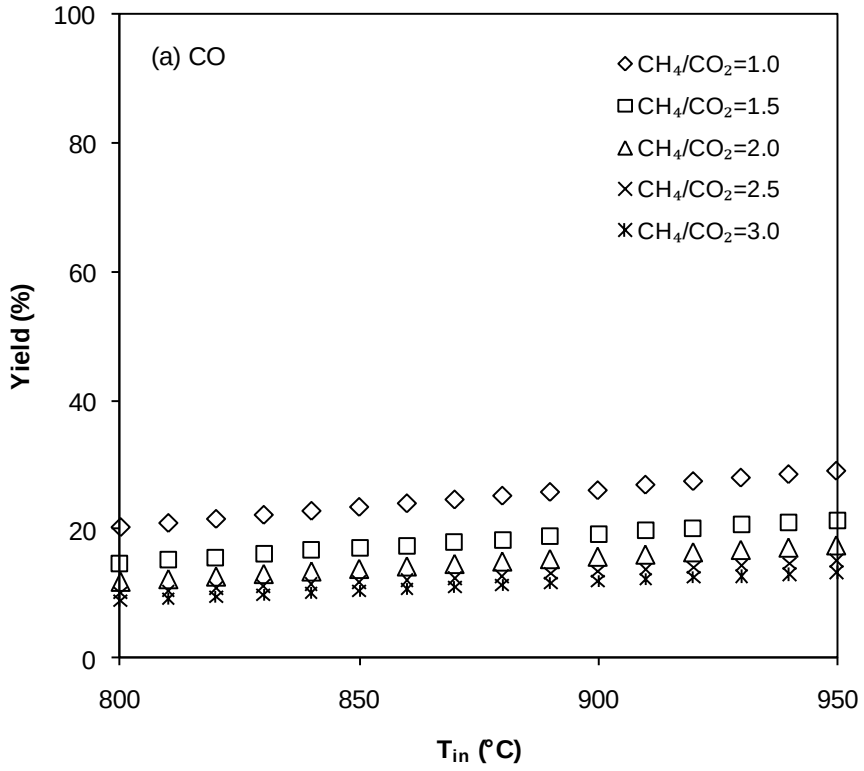

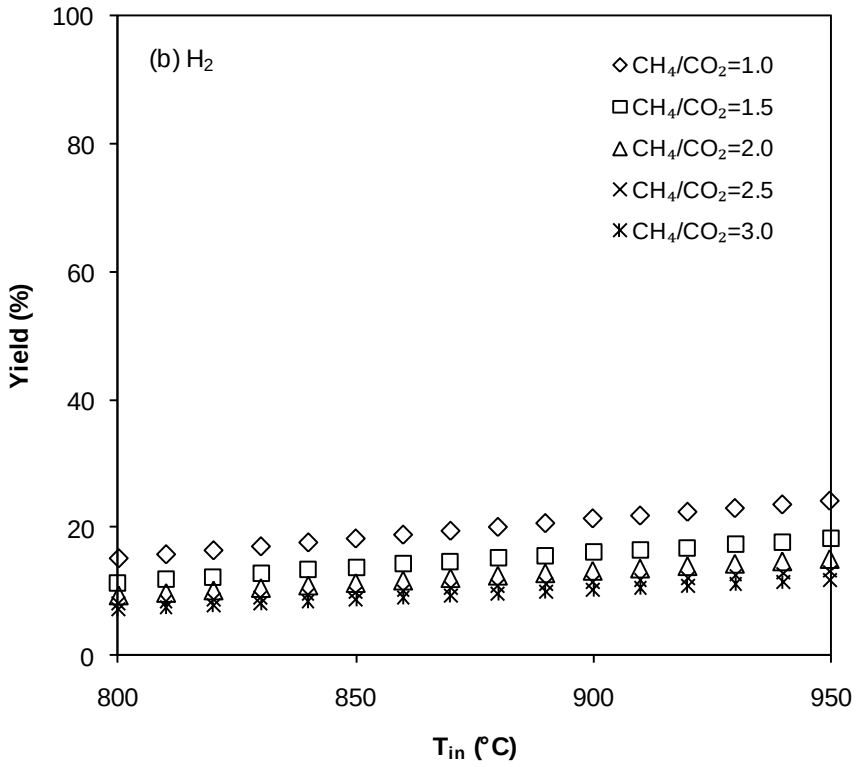

Fig. 11. Prediction of CO and H_2 yields as a function of inlet temperature at different CH_4 to CO_2 ratios. Inlet conditions are given in Fig. 7.

Dependence of H_2 to CO ratio on inlet temperature and CH_4 to CO_2 ratio is displayed in Fig. 12. All H_2 to CO ratios are less than 1.0 and in the range between 0.76 and 0.88. These results indicate the presence of the reverse water-gas shift reaction. Rising of H_2 to CO ratio with inlet temperature indicates that the reverse water-gas shift is less favourable at high temperatures since it is relatively small endothermic comparing with the CH_4 dry reforming.

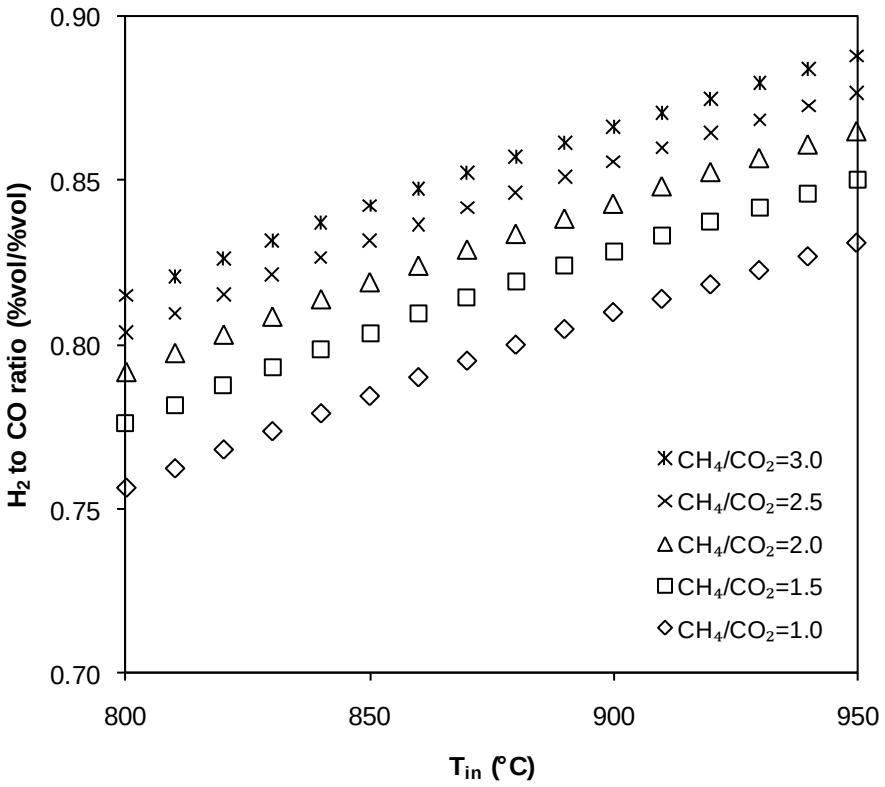

Fig. 12. Prediction of H_2 to CO ratios as a function of inlet temperature at different CH_4 to CO_2 ratios. Inlet conditions are given in Fig. 7**.**

6.2.2. The effect of supplied heat on CH_4 dry reforming activity

In a biogas reforming system without O_2 addition, there are no exothermic reactions (e.g., partial oxidation and complete combustion) taking place. Thus, external energy is necessary (preferably heat that has been wasted such as engine exhaust gas) to drive the dry reforming process. Effects of supplied heat at several CH_4 to CO_2 ratios on gas composition, temperature profile, reactant conversions, product yields, and produced H_2 to CO ratio are given in Figs. 13-17. As presented in Fig. 13, when the supplied heat is increased, enhancement of reaction rates leads to improvement in reactant consumption, Fig. 13(a) and (b), and product generation, Fig. 13(c) and (d). The biogas dry reforming activity is limited by the constant quantity of CO_2, as already mentioned; addition of excess CH_4 (higher CH_4 to CO_2 ratios) results in lower concentrations of CO and H_2.

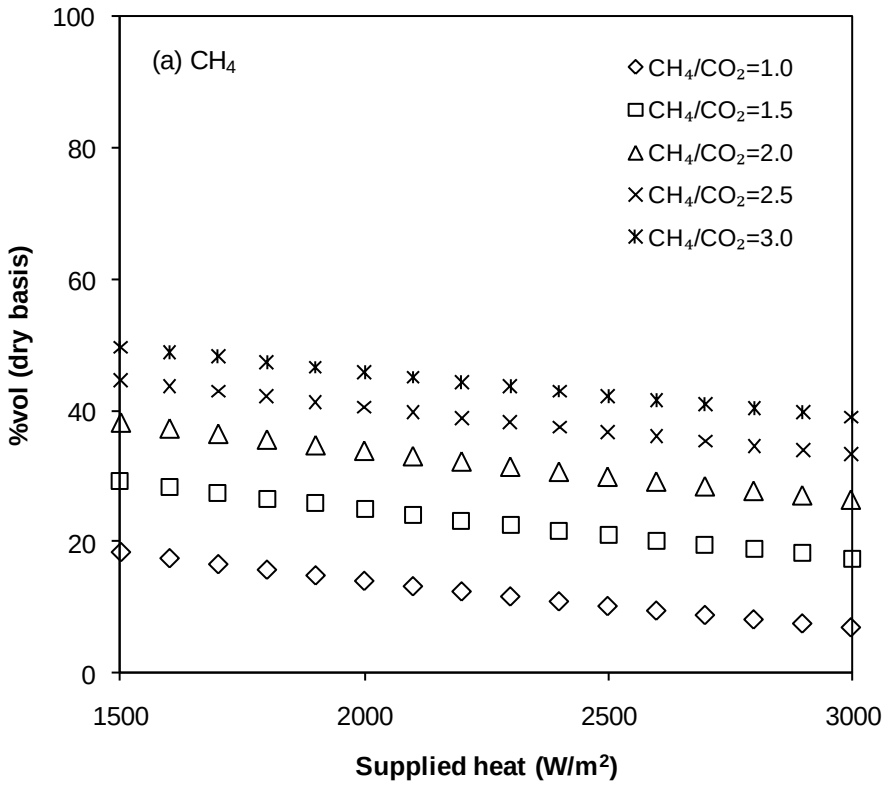
(a) CH4
CH4/CO2=1.0
CH4/CO2=1.5
CH4/CO2=2.0
CH4/CO2=2.5
CH4/CO2=3.0
%vol (dry basis)
Supplied heat (W/m2)
0
20
40
60
80
100
1500
2000
2500
3000

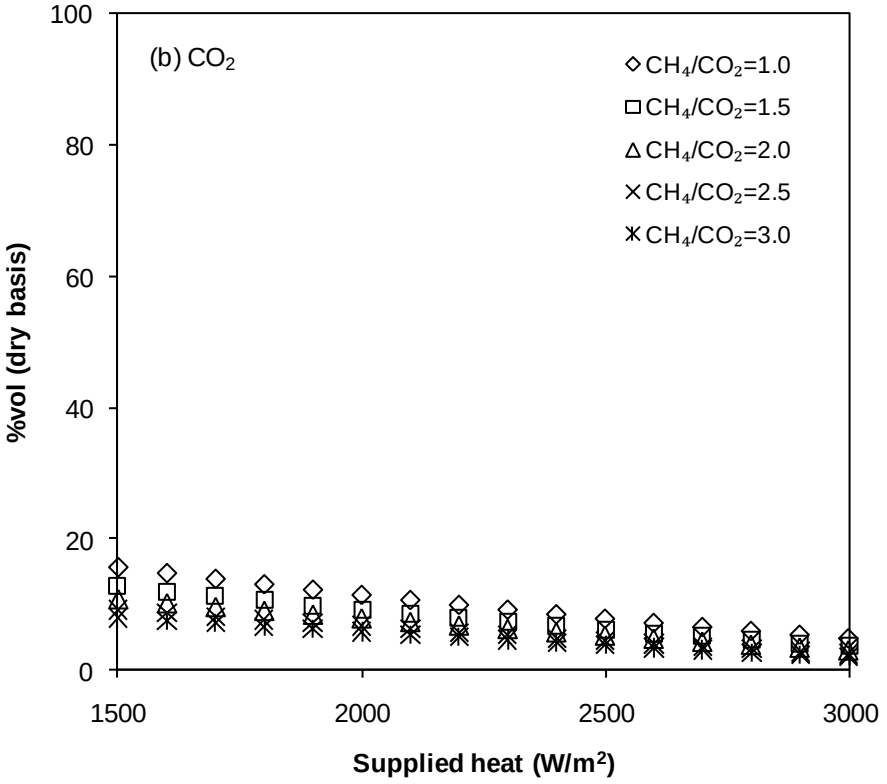
(b) CO2
CH4/CO2=1.0
CH4/CO2=1.5
CH4/CO2=2.0
CH4/CO2=2.5
CH4/CO2=3.0
%vol (dry basis)
Supplied heat (W/m2)
0
20
40
60
80
100
1500
2000
2500
3000

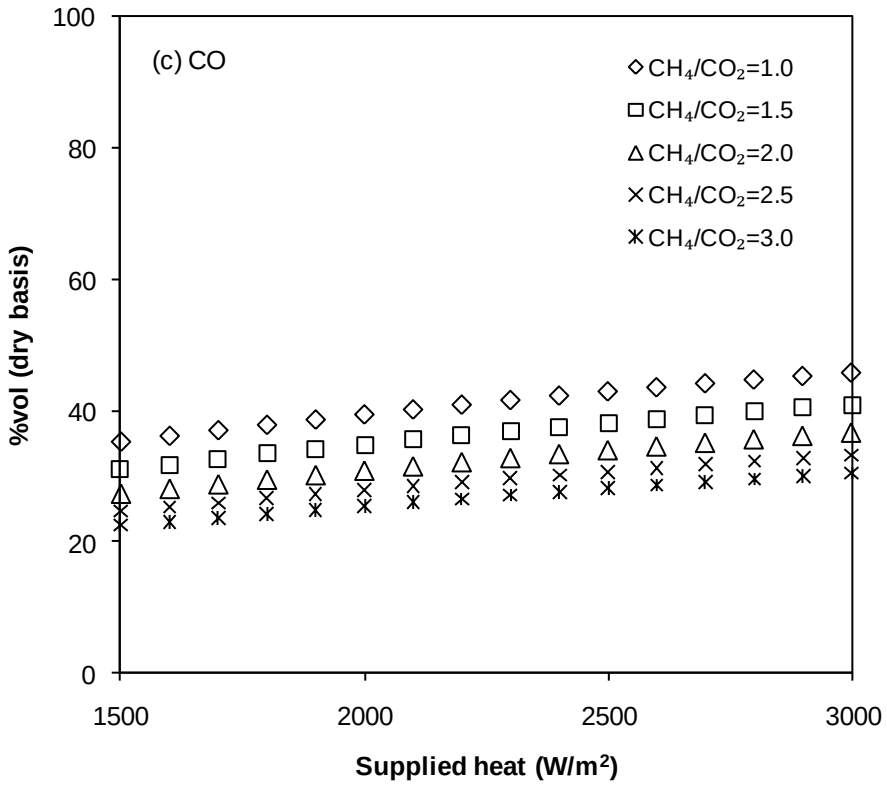

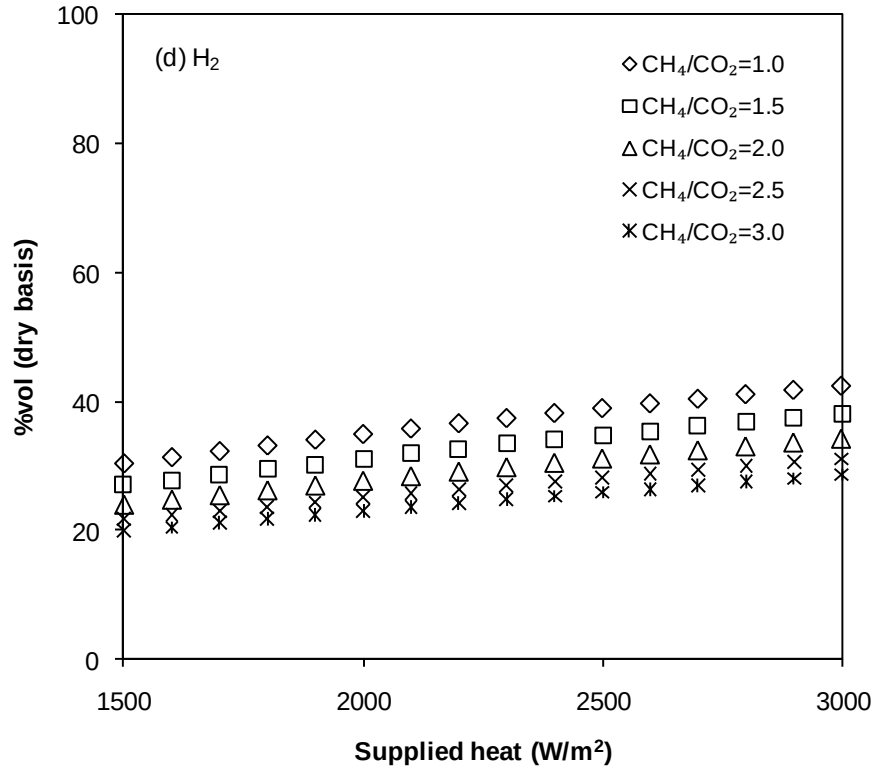

Fig. 13. Model prediction of reactant and product concentrations as a function of supplied heat on reactive wall at different CH_4 to CO_2 ratios. Inlet conditions: constant CO_2 composition of 15 %vol; GHSV of 27500 h^{-1}; inlet temperature of 800 °C.

Effect of supplied heat on temperature profile inside the catalyst is illustrated in Fig. 14. The biogas dry reforming starts immediately at the beginning of catalyst which is characterised by the sharp drop of wall temperature. The nature of endothermic process in this region is noticeable via the lower value of wall temperature comparing with the temperature along the centreline of channel. Interestingly, the value and position of minimum temperatures are nearly independent of supplied heats implying that the chemical reaction of dry reforming is faster than the rate of heat supplied to the system. The end of reforming process is indicated at the point in which wall and axial temperatures are equivalent. Comparison with simulations in the previous section which no external heat provides to the system, the chemical activity is terminated at 25 mm of catalyst length with 615 °C of catalyst temperature in the case of no supplied heat, Fig. 8(a); while, with supplied heat, the dry reforming process finishes at 10 mm and 660 °C. Although the amount of supplied heat does not effect on the terminated characteristics (e.g., position and temperature), the biogas dry reforming activities are dependent on the supplied heat. After the terminated point, supplied heat results in increment of both wall and axial temperatures. Nevertheless, the wall temperature is slightly higher than axial temperature since heat is directly delivered at the catalyst wall.

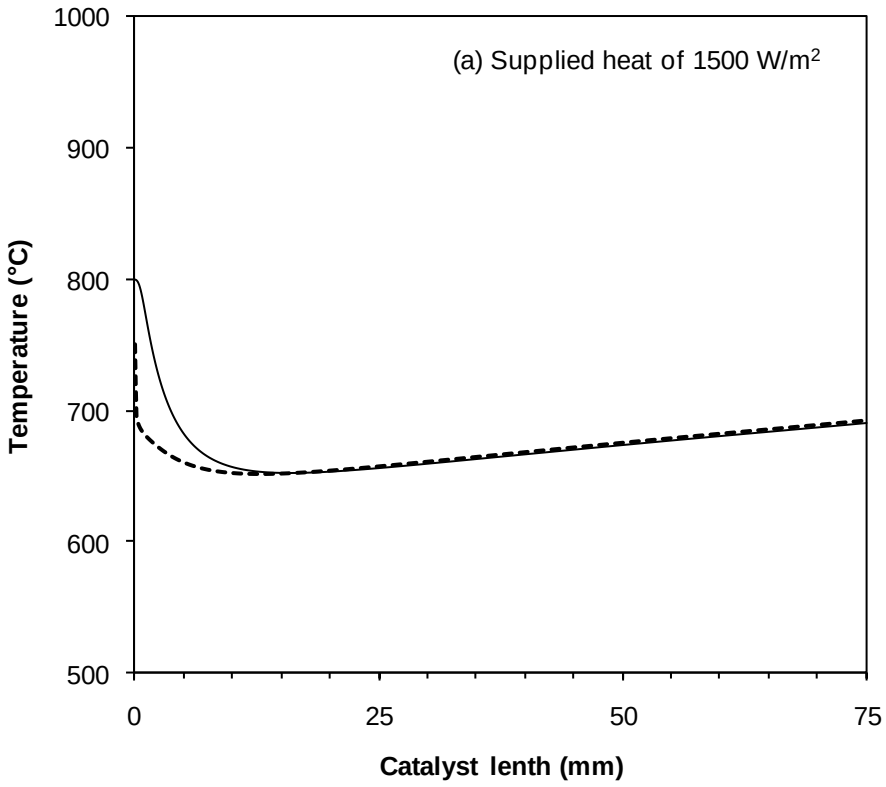
(a) Supplied heat of 1500 W/m2
1000
900
800
700
600
500
Temperature (°C)
0
25
50
75
Catalyst lenth (mm)

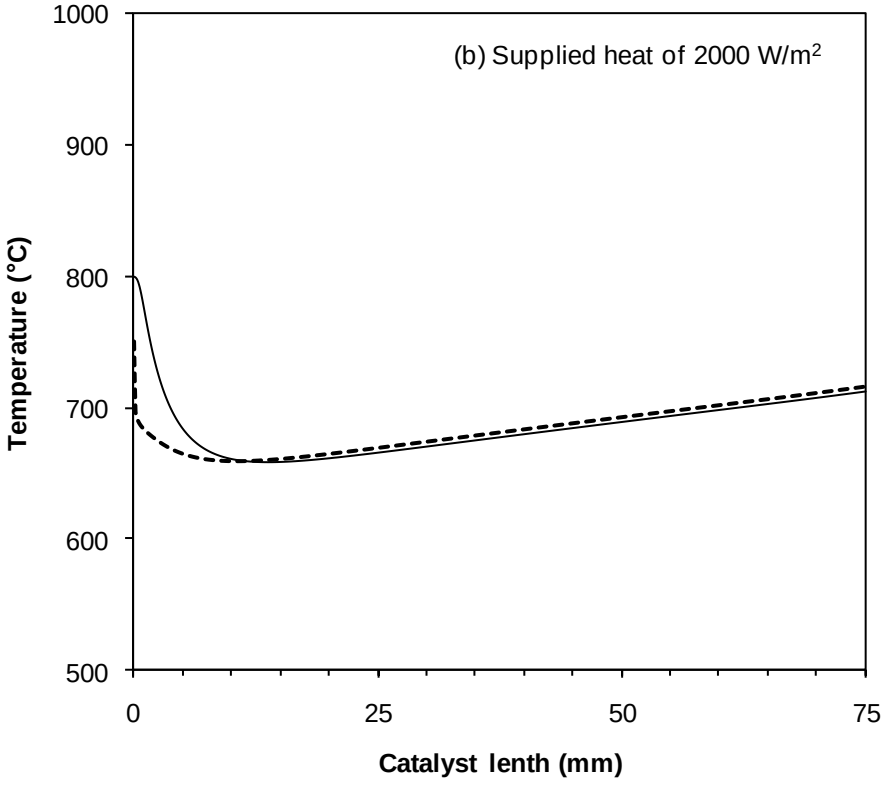
(b) Supplied heat of 2000 W/m2
1000
900
800
700
600
500
Temperature (°C)
0
25
50
75
Catalyst lenth (mm)

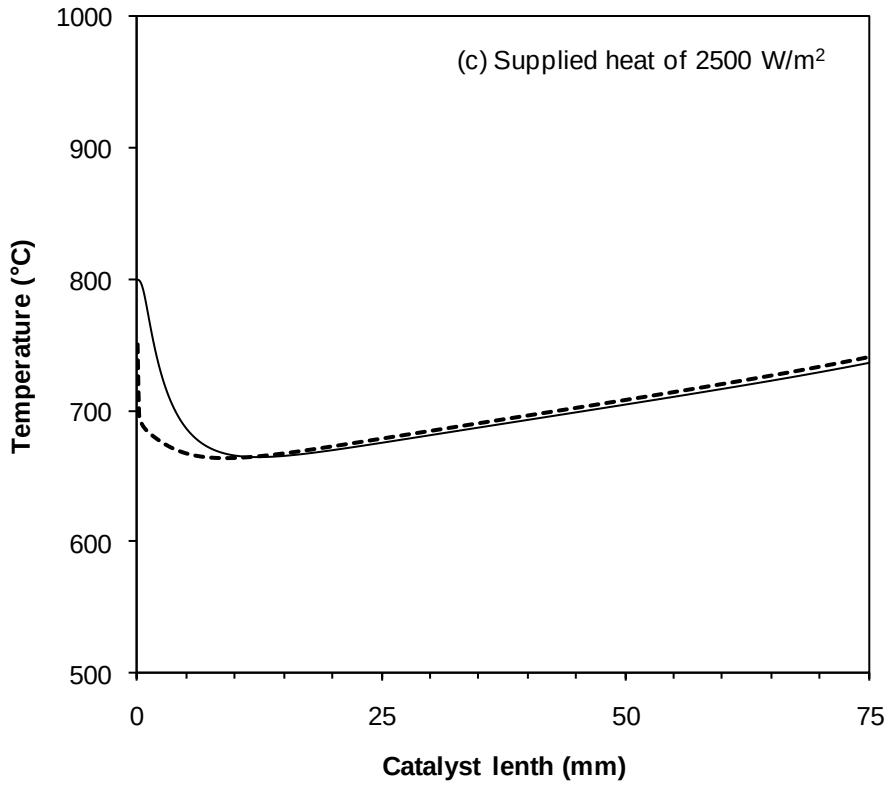

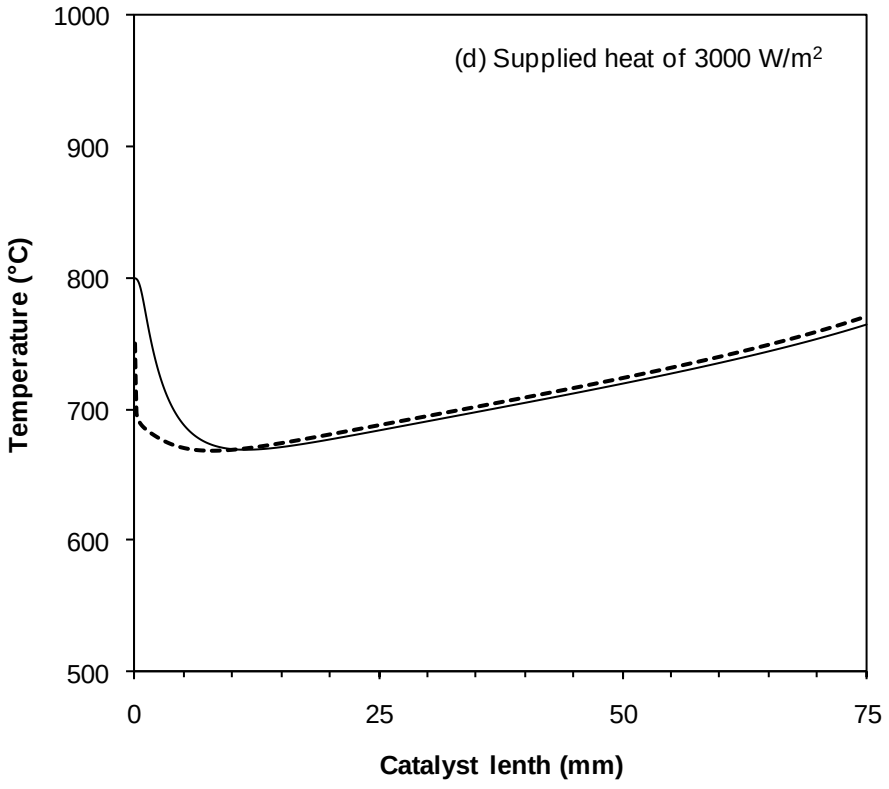

Fig. 14. Temperature profiles inside the catalyst at different supplied heats. Inlet conditions: CO_2 composition of 15 %vol; CH_4 to CO_2 ratio of 1; GHSV of 27500 h^{-1}; inlet temperature of 800 °C. (Solid line: axial temperature. Dash lines: wall temperature.)

Conversions of CH_4 and CO_2 are given in Fig. 15. Role of CO_2 as an important factor to limit the CH_4 dry reforming process is confirmed, as shown in Fig. 15(b), which its conversion is not affected by CH_4 to CO_2 ratios. In general, the CH_4 to CO_2 ratio of natural biogas is between 1 and 3. Therefore, the maximum activity of biogas dry reforming is controlled by the fraction of CO_2. Interestingly, the conversion of CH_4 via dry reforming process has never reached to 100%. This suggests that other reforming methods (e.g., partial oxidation and steam reforming) are required to transform CH_4 completely.

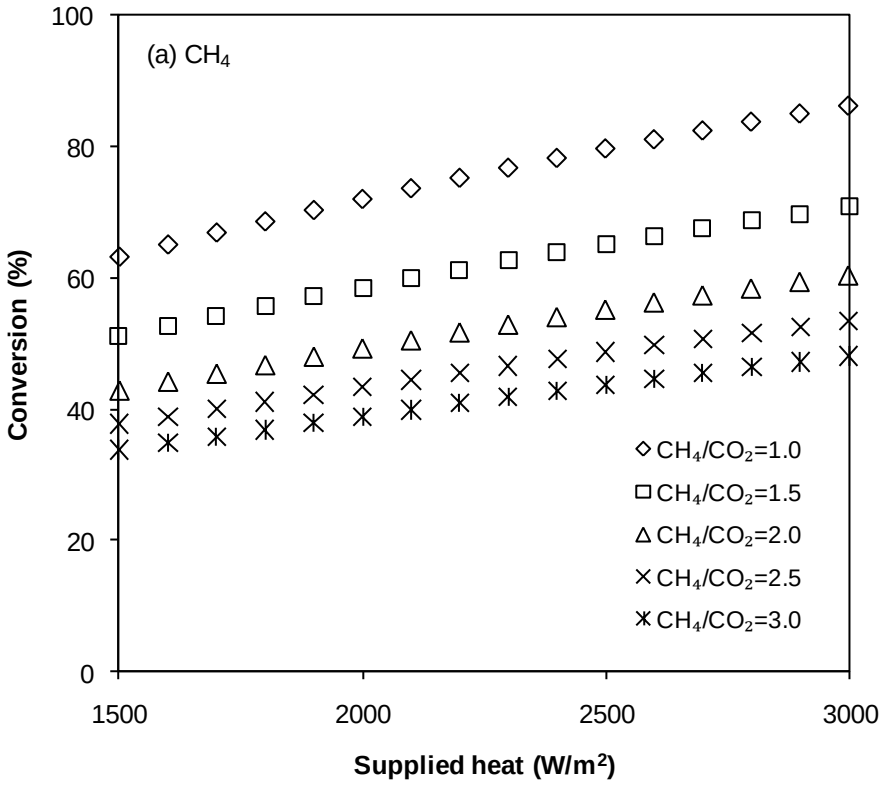

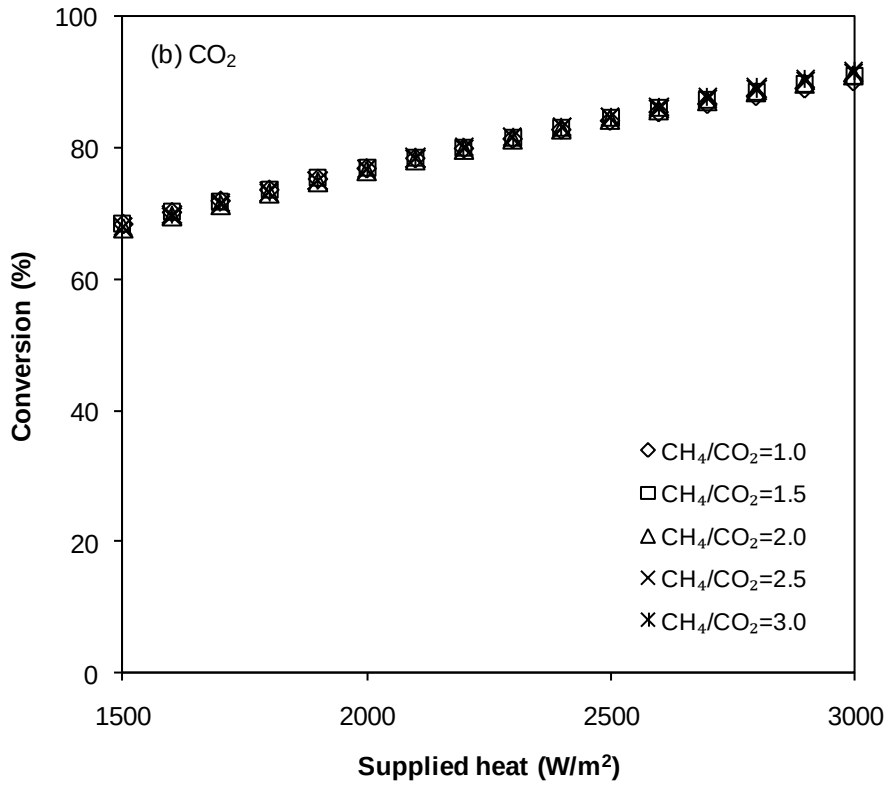

Fig. 15. Prediction of CH_4 and CO_2 conversions as a function of supplied heat on reactive wall at different CH_4 to CO_2 ratios. Inlet conditions are given in Fig. 13.

The effect of supplied heat and CH_4 to CO_2 ratio on product yields is provided in Fig. 16. The increment of un-converse CH_4 as the ratio of CH_4 to CO_2 is raised causes the drop of product yields because the yields are estimated through the amount of inlet CH_4. The side reaction, the reverse water-gas shift, makes the yield of H_2 always lower than that of CO.

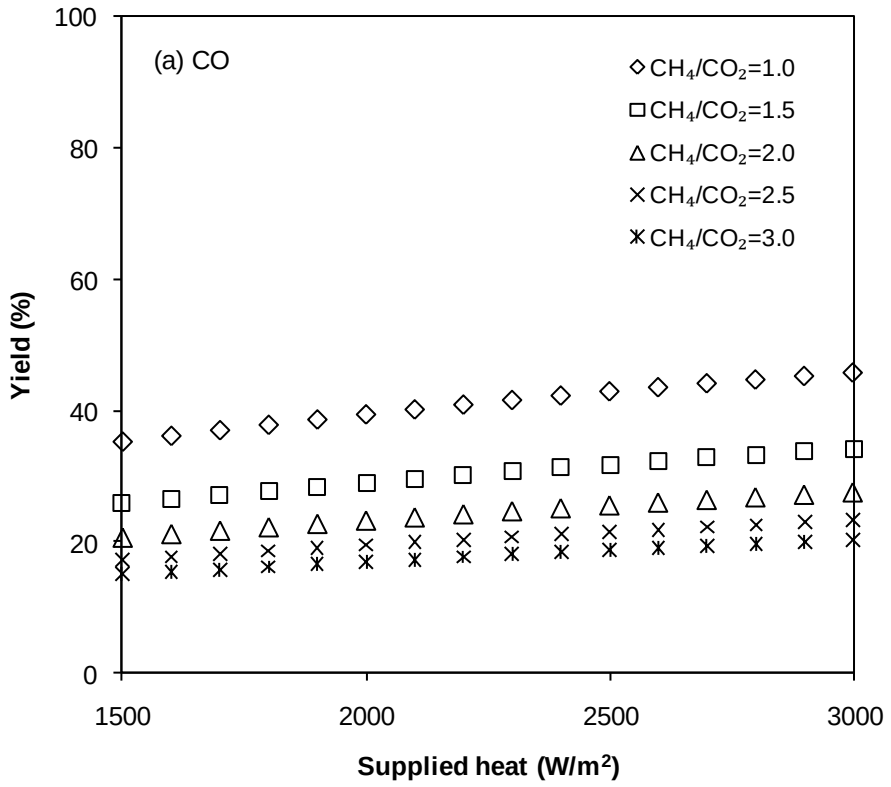

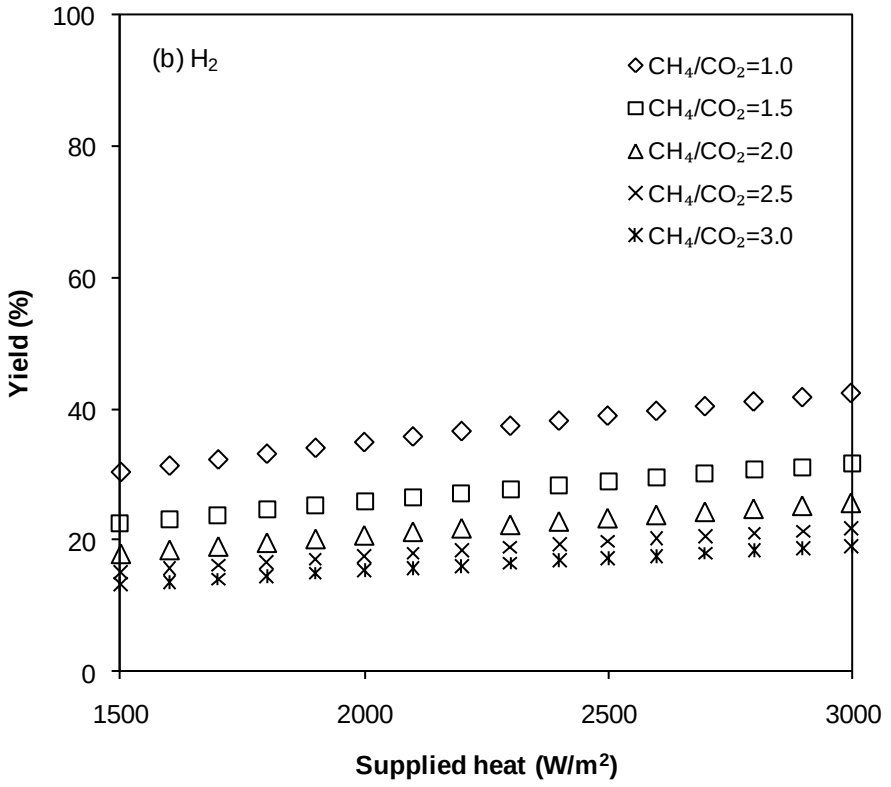

Fig. 16. Yield of CO and H_2 as a function of supplied heat on reactive wall at different CH_4 to CO_2 ratios. Inlet conditions are given in Fig. 13.

The relation of H_2 to CO ratio to supplied heat and inlet CH_4 to CO_2 ratio is explained in Fig. 17. The H_2 to CO ratio depends strongly on supplied heat. Increase of supplied heat promotes the H_2 to CO ratio by decelerating the activity of reverse water-gas shift, as already mentioned in the last section. With supplied heats, the H_2 to CO ratios are between 0.875 and 0.925 while without supplied heat, the ratios are in the range of 0.77 and 0.87. These can be explained by using temperature profiles as shown in Fig. 8 and 14. There are found that with supplied heat, the temperature has never been lower than 660 °C while the temperature is always lower than 640 °C for the reforming without supplied heat. In high operating temperature, the CH_4 dry reforming is promoted and the water gas-shift reaction is suppressed simultaneously; so, higher H_2 to CO ratios are obtained.

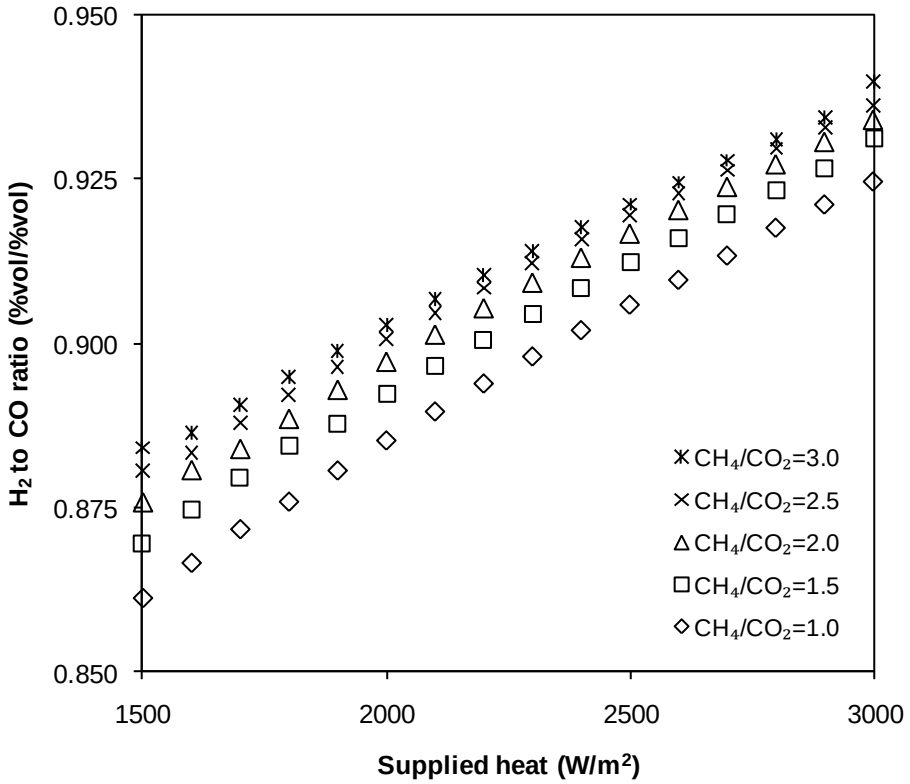

Fig. 17. Prediction of H_2 to CO ratios as a function of supplied heat on reactive wall at different CH_4 to CO_2 ratios. Inlet conditions are given in Fig. 13.

The activity of biogas dry reforming including reactant conversions, product yields, and temperature profiles as a function of inlet temperature, supplied heat, and CH_4 to CO_2 ratio has been presented in previous sections. For a specific value of CH_4 to CO_2 ratio, the model can be utilised to design a biogas reforming system with suitable inlet temperature and supplied heat to provide desired product yields and catalyst temperature that the catalytic materials can be tolerated. The model also shows that there are always existences of unconverted CO_2 due to thermodynamic limitation and CH_4 which is limited by the less amount of CO_2. Thus, to deal with the remaining CH_4, other reforming processes are adopted together with the dry reforming. To construct a fuel reforming system for using in an automotive aftertreatment, external supplied heat is first provided from exhaust gas. Moreover, the main supplied heat is produced from both partial oxidation and complete combustion by adding a controlled value of O_2 into the system. At this circumstance, the endothermic dry reforming is one of parameters used to prevent too high operating temperature. Finally, the model of dry reforming is expected to be applied with other fuel reforming models (e.g., partial oxidation, complete combustion, steam reforming, and water-gas shift), which will be created later to design an effective biogas reforming system for on-board a vehicle processes.

7. Conclusion

Simulation for catalytic biogas dry reforming over a single channel of a monolithic platinum-rhodium alumina catalyst is presented in this work. Based on combination of LHHW and microkinetic modelling approaches, a compact mechanism consisting of CH_4 dry reforming and reverse water-gas shift reactions is formulated. The LHHW method is applied to form rate expressions while microkinetics is utilised to estimate activation energies. As always accompanied with the LHHW rate expression, equilibrium constants for adsorption and desorption processes of various gases are calculated by using the transition state theory. It is found that the Langmuir-Hinshelwood surface reaction is the rate determining step when the reforming process proceeds in relatively high operating temperature range; whereas in

relatively low temperature range, the dissociative adsorption of CH_4 is the rate controlling step. The proposed mechanism is optimised and validated against experimental data at different operating conditions (e.g., temperatures and space velocities). The proposed model is able to predict the effect of inlet temperature, supplied heat, and inlet CH_4 to CO_2 ratio on conversion of CH_4 and CO_2, production of CO and H_2, produced H_2 to CO ratio, and temperature profile inside the catalyst with reasonable precision.

Acknowledgments

College of Industrial Technology at King Mongkut's University of Technology North Bangkok is gratefully acknowledged for financial support.

References

[1] Theinnoi K, Tsolakis A, Sitshebo S, Cracknell RF, Clark RH. Fuels combustion effects on a passive mode silver/alumina HC-SCR catalyst activity in reducing NOx. Chem Eng J 2010;158:468–73. doi:http://dx.doi.org/10.1016/j.cej.2010.01.021.

[2] Sitshebo S, Tsolakis A, Theinnoi K. Promoting hydrocarbon-SCR of NOx in diesel engine exhaust by hydrogen and fuel reforming. Int J Hydrogen Energy 2009;34:7842–50. doi:http://dx.doi.org/10.1016/j.ijhydene.2009.07.059.

[3] Sitshebo S, Tsolakis A, Theinnoi K, Rodríguez-Fernández J, Leung P. Improving the low temperature NOx reduction activity over a Ag-Al2O3 catalyst. Chem Eng J 2010;158:402–10. doi:http://dx.doi.org/10.1016/j.cej.2010.01.004.

[4] Rodríguez-Fernández J, Tsolakis A, Cracknell RF, Clark RH. Combining GTL fuel, reformed EGR and HC-SCR aftertreatment system to reduce diesel NOx emissions. A statistical approach. Int J Hydrogen Energy 2009;34:2789–99. doi:http://dx.doi.org/10.1016/j.ijhydene.2009.01.026.

[5] Theinnoi K, Gill SS, Tsolakis A, York A. PE, Megaritis A, Harrison RM. Diesel Particulate Filter Regeneration Strategies: Study of Hydrogen Addition on Biodiesel Fuelled Engines. Energy & Fuels 2012;26:1192–201. doi:10.1021/ef201355b.

[6] Tsolakis A, Megaritis A, Wyszynski ML. Application of Exhaust Gas Fuel Reforming in Compression Ignition Engines Fueled by Diesel and Biodiesel Fuel Mixtures. Energy & Fuels 2003;17:1464–73. doi:10.1021/ef0300693.

[7] Tsolakis A, Megaritis A, Wyszynski M. Low temperature exhaust gas fuel reforming of diesel fuel. Fuel 2004;83:1837–45. doi:10.1016/j.fuel.2004.03.012.

[8] Abu-Jrai A, Rodríguez-Fernández J, Tsolakis A, Megaritis A, Theinnoi K, Cracknell RF, et al. Performance, combustion and emissions of a diesel engine operated with reformed EGR. Comparison of diesel and GTL fuelling. Fuel 2009;88:1031–41. doi:http://dx.doi.org/10.1016/j.fuel.2008.12.001.

[9] Ishida M, Yamamoto S, Ueki H, Sakaguchi D. Remarkable improvement of NOx–PM trade-off in a diesel engine by means of bioethanol and EGR. Energy 2010;35:4572–81. doi:http://dx.doi.org/10.1016/j.energy.2010.03.039.

[10] Banerjee R, Roy S, Bose PK. Hydrogen-EGR synergy as a promising pathway to meet the PM–NOx–BSFC trade-off contingencies of the diesel engine: A comprehensive review. Int J Hydrogen Energy 2015;40:12824–47. doi:http://dx.doi.org/10.1016/j.ijhydene.2015.07.098.

[11] Fennell D, Herreros J, Tsolakis A. Improving gasoline direct injection (GDI) engine efficiency and emissions with hydrogen from exhaust gas fuel reforming. Int J Hydrogen Energy 2014;39:5153–62. doi:https://doi.org/10.1016/j.ijhydene.2014.01.065.

[12] Bogarra M, Herreros JM, Tsolakis A, York APE, Millington PJ. Study of particulate matter and gaseous emissions in gasoline direct injection engine using on-board exhaust gas fuel reforming. Appl Energy 2016;180:245–55. doi:https://doi.org/10.1016/j.apenergy.2016.07.100.

[13] Bogarra M, Herreros JM, Tsolakis A, York APE, Millington PJ, Martos FJ. Impact of exhaust gas fuel reforming and exhaust gas recirculation on particulate matter morphology in Gasoline Direct Injection Engine. J Aerosol Sci 2017;103:1–14. doi:https://doi.org/10.1016/j.jaerosci.2016.10.001.

[14] Lau CS, Tsolakis A, Wyszynski ML. Biogas upgrade to syn-gas (H2–CO) via dry and oxidative reforming. Int J Hydrogen Energy 2011;36:397–404. doi:10.1016/j.ijhydene.2010.09.086.

[15] Lau CS, Allen D, Tsolakis A, Golunski SE, Wyszynski ML. Biogas upgrade to syngas through thermochemical recovery using exhaust gas reforming. Biomass and Bioenergy 2012;40:86–95. doi:http://dx.doi.org/10.1016/j.biombioe.2012.02.004.

[16] Rathod V, Bhale P V. Experimental Investigation on Biogas Reforming for Syngas Production over an Alumina based Nickel Catalyst. Energy Procedia 2014;54:236–45. doi:http://dx.doi.org/10.1016/j.egypro.2014.07.267.

[17] Bereketidou OA, Goula MA. Biogas reforming for syngas production over nickel supported on ceria–alumina catalysts. Catal Today 2012;195:93–100. doi:10.1016/j.cattod.2012.07.006.

[18] Passos FB, Oliveira ER, Mattos L V., Noronha FB. Effect of the support on the mechanism of partial oxidation of methane on platinum catalysts. Catal Letters 2006;110:161–7. doi:10.1007/s10562-006-0105-z.

[19] Sadykov VA, Gubanova EL, Sazonova NN, Pokrovskaya SA, Chumakova NA, Mezentseva NV, et al. Dry reforming of methane over Pt/PrCeZrO catalyst: Kinetic and mechanistic features by transient studies and their modeling. Catal Today 2011;171:140–9. doi:10.1016/j.cattod.2011.04.004.

[20] Ay H, Üner D. Dry reforming of methane over CeO2 supported Ni, Co and Ni–Co catalysts. Appl Catal B Environ 2015;179:128–38. doi:http://dx.doi.org/10.1016/j.apcatb.2015.05.013.

[21] Wang S, Lu GQ (Max), Millar GJ. Carbon Dioxide Reforming of Methane To Produce Synthesis Gas over Metal-Supported Catalysts: State of the Art. Energy & Fuels 1996;10:896–904. doi:10.1021/ef950227t.

[22] O'Connor AM, Schuurman Y, Ross JRH, Mirodatos C. Transient studies of carbon dioxide reforming of methane over Pt/ZrO2 and Pt/Al2O3. Catal Today 2006;115:191–8.

doi:10.1016/j.cattod.2006.02.051.

[23] Djinović P, Batista J, Pintar A. Efficient catalytic abatement of greenhouse gases: Methane reforming with CO_2 using a novel and thermally stable Rh–CeO_2 catalyst. Int J Hydrogen Energy 2012;37:2699–707. doi:10.1016/j.ijhydene.2011.10.107.

[24] Behroozsarand A, Pour AN. Modeling of microreactor for methane dry reforming: Comparison of Langmuir–Hinshelwood kinetic and microkinetic models. J Nat Gas Sci Eng 2014;20:99–108. doi:10.1016/j.jngse.2014.06.011.

[25] Nematollahi B, Rezaei M, Asghari M, Fazeli A, Lay EN, Nematollahi F. A comparative study between modeling and experimental results over rhodium supported catalyst in dry reforming reaction. Fuel 2014;134:565–72. doi:10.1016/j.fuel.2014.05.093.

[26] Kumar S, Agrawal M, Kumar S, Jilani S. The Production of Syngas by Dry Reforming in Membrane Reactor Using Alumina-Supported Rh Catalyst: A Simulation Study. Int J Chem React Eng 2008;6. doi:10.2202/1542-6580.1803.

[27] Donazzi A, Beretta A, Groppi G, Forzatti P. Catalytic partial oxidation of methane over a 4% Rh/α-Al2O3 catalyst Part II: Role of CO2 reforming. J Catal 2008;255:259–68. doi:http://dx.doi.org/10.1016/j.jcat.2008.02.010.

[28] Maestri M, Vlachos DG, Beretta A, Groppi G, Tronconi E. Steam and dry reforming of methane on Rh: Microkinetic analysis and hierarchy of kinetic models. J Catal 2008;259:211–22. doi:http://dx.doi.org/10.1016/j.jcat.2008.08.008.

[29] Koehle M, Mhadeshwar A. Microkinetic modeling and analysis of ethanol partial oxidation and reforming reaction pathways on platinum at short contact times. Chem Eng Sci 2012;78:209–25. doi:10.1016/j.ces.2012.05.017.

[30] Dumesic JA, Rudd DF, Aparicio LM, Rekoske JE, Treviño AA. The Microkinetics of heterogeneous catalysis. American Chemical Society; 1993.

[31] Shustorovich E. The UBI-QEP method: A practical theoretical approach to understanding chemistry on transition metal surfaces. Surf Sci Rep 1998;31:1–119. doi:10.1016/S0167-5729(97)00016-2.

[32] Sellers H, Shustorovich E. Intrinsic activation barriers and coadsorption effects for reactions on metal surfaces: unified formalism within the UBI-QEP approach. Surf Sci 2002;504:167–82. doi:10.1016/S0039-6028(01)02025-8.

[33] Shustorovich E, Zeigarnik A V. The UBI–QEP treatment of polyatomic molecules without bond-energy partitioning. Surf Sci 2003;527:137–48. doi:10.1016/S0039-6028(03)00013-X.

[34] Kraus P, Lindstedt RP. Microkinetic Mechanisms for Partial Oxidation of Methane over Platinum and Rhodium. J Phys Chem C 2017;121:9442–53. doi:10.1021/acs.jpcc.7b02397.

[35] Wei J, Iglesia E. Structural requirements and reaction pathways in methane activation and chemical conversion catalyzed by rhodium. J Catal 2004;225:116–27. doi:http://dx.doi.org/10.1016/j.jcat.2003.09.030.

[36] Niu J, Du X, Ran J, Wang R. Dry (CO2) reforming of methane over Pt catalysts studied by DFT and kinetic modeling. Appl Surf Sci 2016;376:79–90. doi:http://dx.doi.org/10.1016/j.apsusc.2016.01.212.

[37] Dumesic JA, Huber GW, Boudart M. Microkinetics. In: Ertl G, Knozinger H, Schuth F, Weitkamp J, editors. Handb. Heterog. Catal. 2nd ed., Wiley VCH; 2008, p. 1445–62.

[38] Hayes RE, Kolaczkowski ST. Introduction to Catalytic Combustion. CRC Press; 1998.

[39] Aghalayam P, Park YK, Vlachos DG. Construction and optimization of complex surface-reaction mechanisms. AIChE J 2000;46:2017–29. doi:10.1002/aic.690461013.